Models confirm that recent European wildfires are exacerbated by anthropogenic climate change

Chen Lu, Rita Nogherotto, Tommaso Alberti, Gabriele Messori, Erika Coppola, Davide Faranda

Models Confirm that Recent European Wildfires Are Exacerbated by Anthropogenic Climate Change

Chen Lu[1], Rita Nogherotto[1,2], Tommaso Alberti[3], Gabriele Messori[4,5,6], Erika Coppola[1], Davide Faranda[7,8,9]

[1] The Abdus Salam International Centre for Theoretical Physics, Trieste, Italy
[2] Istituto di Scienze Atmosferiche e Clima, CNR, Bologna, Italy
[3] Istituto Nazionale di Geofisica e Vulcanologia, Rome, Italy
[4] Department of Earth Sciences, Uppsala University, Uppsala, Sweden
[5] Swedish Centre for Impacts of Climate Extremes (climes), Uppsala University, Uppsala, Sweden
[6] Department of Meteorology and Bolin Centre for Climate Research, Stockholm University, Stockholm, Sweden
[7] Laboratoire des Sciences du Climat et de l'Environnement, UMR 8212 CEA-CNRS-UVSQ, Université Paris-Saclay & IPSL, CE Saclay l'Orme des Merisiers, 91191, Gif-sur-Yvette, France
[8] London Mathematical Laboratory, 8 Margravine Gardens, London, W6 8RH, British Islands
[9] Laboratoire de Météorologie Dynamique/IPSL, École Normale Supérieure, PSL Research University, Sorbonne Université, École Polytechnique, IP Paris, CNRS, 75005, Paris, France

E-mail: clu@ictp.it

6 November 2024

Abstract. Climate change is an ongoing process that is modifying weather patterns and influencing weather phenomena and extreme events such as heatwaves, droughts, and floods. This paper investigates whether climate change can also play a role in enhancing wildfires by focusing on a set of three recent wildfires in Europe. We employ the concept of analogues to assess the influence of climate change on the atmospheric conditions underlying wildfire development monitored through the fire weather index, by comparing past and present atmospheric patterns similar to those that occurred during the wildfire. Our analysis focuses on both reanalysis data and high-resolution regional climate models to verify the observed changes and provide future projections. Our findings show that climate change has altered critical factors supporting wildfire development, such as wind patterns, temperature, and humidity. The results from our sample of three events point out that climate change has increased wildfire hazards in Europe, which is projected to further increase for similar fire weather conditions in the future.

Keywords: Wildfires - Atmospheric circulation - Climate Change - Attribution - Regional climate model - CORDEX

1. Introduction

As climate change intensifies, wildfires have transitioned from being sporadic occurrences to recurring crises [1, 2]. Weather stands out as a key factor governing regional burned area. Atmospheric circulation patterns and meteorological variables such as wind speed and direction, temperature, and humidity are crucial in both the ignition and spread of fires [3], although available fuel and potential ignition sources are also needed [4]. Europe is no exception to the global trend towards higher burned area and increased occurrence/magnitude, which has been linked to the compound increase of droughts and heatwaves, and the resulting high temperatures and low soil moisture [5, 6]. Specifically, the IPCC states that there is medium confidence that fire weather conditions in Southern Europe have become more likely in the last century and high confidence that they will increase in the future for global warming of 2 degrees and above [7, 5].

The increase in weather conditions favoring wildfire is part of broader climate system changes associated with anthropogenic climate change [8]. While long-term trends in weather events can often be attributed to climate change with high confidence, attributing individual events remains challenging. There is a growing number of approaches for attribution analyses [9, 10, 11, 12, 13], yet these often come with considerable uncertainty, and event attribution is the subject of ongoing debate [14, 15]. Consequently, while trends in fire danger have been studied [16, 1], wildfire attribution studies are scant.

This paper employs atmospheric analogues to elucidate the weather conditions associated with three recent wildfires in Europe, specifically in Central Sweden (July 2018), France (summer 2022), and Sicily and Greece (July 2023), in both reanalysis and model data. Here we use an approach based on atmospheric analogues, which hold promise for attributing extreme weather events to underlying climate change conditions by comparing current atmospheric patterns with those from historical records [17, 18]. This can help us assess whether climate change to date has led to conditions more conducive to wildfires. The atmospheric analogues and the associated fire weather conditions in high-resolution regional climate models (RCMs) are further examined, which can help confirm the observed changes and provide future projections.

2. Data & Methods

2.1. Data

We analyse daily ERA5 reanalysis data [19] with a horizontal grid resolution 0.25° × 0.25°, from 01-Jan-1950 to 31-Jul-2023. Two European domains are considered: 20 W°-30°E, 30°N-60°N and 5 E°-30°E, 50°N-70°N. We use 500 hPa geopotential height (z500) to identify analogues. To assess the risk of wildfire ignition and spread based on multiple meteorological and environmental factors, we use the Fire Weather Index (FWI) produced by the Copernicus Emergency Management Service for the European Forest Fire Information System (EFFIS) ([20]). This index was developed by the Canadian

Forest Service in the 1970s [21, 22]. A higher value in FWI indicates conditions more favourable for sustaining a fire once one is ignited.

RCM data from the Coordinated Regional Climate Downscaling Experiment (CORDEX) are also examined in this study [23, 9, 24]. We consider a total of 31 scenario simulations from the CORDEX European Domain with 0.11° resolution (EUR-11) driven by global climate models, details of which are shown in Table S1. The historical and RCP8.5 scenarios are considered, with the former covering the period of 1980-2005, and the latter 2006-2098. FWI in the models are derived using relative humidity (rh), daily accumulated precipitation (tp), maximum 2-meter temperature (tmax), and maximum 10-meter wind speed(wspdmax). The obtained FWI, together with z500, 2-meter temperature (t2m), and 10-meter wind speed (wspd) are then preprocessed following the same procedure as used for ERA5.

2.2. Analogs attribution method

Following [17], we explore the role of anthropogenic climate change on the occurrence of European wildfires by comparing the analogues during the 1950-1979 period to those from 1992-2021 (hereafter referred to as the full analysis). We assume that the first period represents a counterfactual (CF) world, where a weak to moderate anthropogenic influence on climate is present, while the latter represents a factual (F) world, with an increased role of anthropogenic-induced climate change. Analogue-based assignment (e.g., [25, 17, 26]) relies on the definition of a *target event* to be compared with a set of other events/conditions. In our case, the *target event* is the z500 pattern associated with wildfires observed over a specific region and with a certain duration in time (i.e., number of days). The area and duration of the *target event* are determined based on both its socioeconomic impacts and the location and extent of the meteorological drivers, following the approach by ClimaMeter (www.climameter.org) [18].

The analogues are identified based on the Euclidean distance $d(\mathbf{Ev}, \mathbf{Y})$ between the *target event* ($\mathbf{Ev}$) and the remaining z500 maps ($\mathbf{Y}$). We select the best 22 patterns ($\sim$0.6% days) that minimize $d(\mathbf{Ev}, \mathbf{Y})$ in the extended season of the *target event*. With the identified analogues, the composites in the CF/F periods, the changes between the two, and the analogues metrics (including the analogue quality Q, the instantaneous dimension D, and the persistence Θ) can be calculated. It is worth-mentioning that Q indicates how unique a *target event* is, and the level of confidence we can place in our analogues approach. We further evaluate the impact of natural climate variability (including the El Niño-Southern Oscillation (ENSO), the Atlantic Multidecadal Oscillation (AMO), and the Pacific Decadal Oscillation (PDO)) on the *target event* by testing for significant changes between their CF/F probability distribution functions. We additionally determine the top 54 analogues ($\sim$0.6% days) for the entire time interval and examine the variation in their frequency by gauging a linear trend. A detailed description of the definitions and implications of these metrics, as well as the tests for statistical significance, is provided in the supplementary materials.

2.3. Bias correction, model evaluation and projection

The analogues attribution in CORDEX is undertaken on both the raw and the bias-corrected z500. The bias correction method employed is the Cumulative Distribution Function – transform (CDF-t) method, developed by Michelangeli et al. [27]. The calculation is carried out using the "CDF-t" R package [28].

Model-based changes in z500 and FWI (obtained from the analogues analysis) are compared with the ERA5-based ones. The analyses are undertaken over the common period of RCM and ERA5, and the counterfactual and factual periods are chosen as 1980-1999 and 2001-2020, respectively, each containing 20 years (hereafter referred to as the validation analysis).

To better estimate future changes, the models are selected based on their skills in simulating event-day z500 patterns. As the days in RCM do not correspond with the actual calendar days, the event-day patterns are not defined in the models; therefore, the event-day ERA5 patterns is used for analogues identification, and the obtained analogues in model data are used as a proxy for model performance. Specifically, for each RCM, the correlation coefficients between the event-day pattern in ERA5 and the analogues identified in RCM from both counterfactual and factual periods are calculated. The average value of the correlation coefficients is used as an indicator of model skill. The average correlation coefficients between ERA5 analogues and event-day z500 patterns (0.900, 0.763, and 0.906 for the three cases) is used as the selection standard. In addition, we consider models with slightly lower skill, i.e., 0.05 less than the ERA5 correlation, having adequate performance to be included in the ensemble.

Future changes in FWI are evaluated in both near and far future. The counterfactual period is 1980-2009 for both, and the factual periods are 2022-2051 and 2069-2098, respectively. Ensemble mean of changes in z500 and FWI are presented. The statistical significance of change is evaluated based on a two-sided t-test with a significance level of 0.05, and we also applied the Benjamini & Hochberg procedure [29] for controlling the false discovery rate as multiple testing correction [30, 31]; the results of the latter are similar to those of the former in most of the cases. Additionally, model agreement is evaluated; consistent change is considered if over 80% of the ensemble members agree on the sign [32]. For each event, the average changes in FWI are also evaluated over the area most affected, which are defined by the gray boxes shown in Figure 1. Statistical significance in whether ensemble mean and median changes are different from 0 is determined based on one-sample t-test and Wilcoxon signed rank test.

3. Results

3.1. 2023/07/25 Sicily and Greece wildfires

Summer 2023 is a season of heatwaves in the Mediterranean [34]. It has witnessed a series of impactful wildfires, with Sicily and Greece experiencing some of the most severe

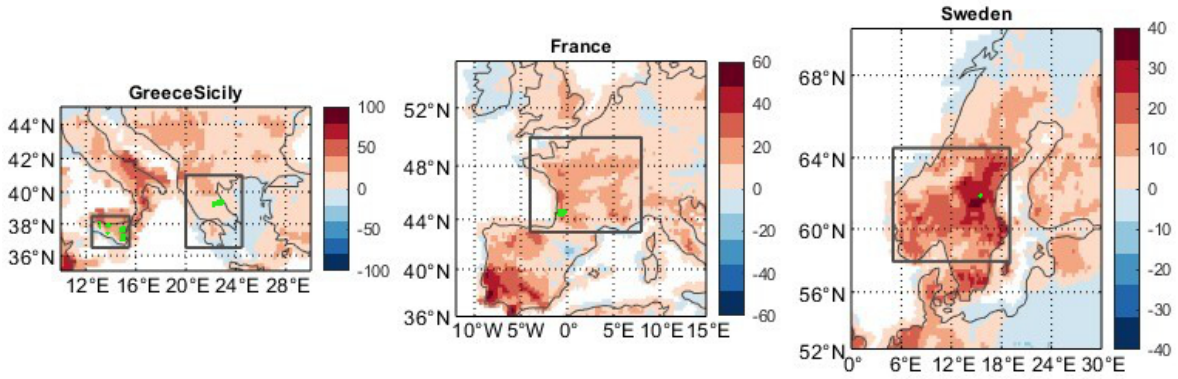

Figure 1. Fire weather index anomalies (with respect to a reference period of 1950-2023) on the event day for the three events. The gray boxes mark the area used for calculating the area average changes. The location of the wildfires (obtained from Global Wildfire Information System [33]) is marked by the green hatches.

on record. In Sicily, wildfires started on 25 July, isolating its major cities, Catania and Palermo, causing power and water shortages. This resulted in a state of emergency declaration from the Italian Government. The EFFIS Joint Research Centre (`https://effis.jrc.ec.europa.eu/about-effis`) reported over 5,000 hectares burnt, with an estimated €250 million to address agricultural damage [35]. In Greece, wildfires caused at least 28 deaths, injured 75, and led to mass evacuations, forcing the government to establish a Crisis Management Unit.

Figure 2 shows the results of the attribution of the atmospheric circulation configuration associated with the Sicily and Greece wildfires based on ERA5 and CORDEX data. (Detailed results of the ERA5 full analysis, including those for Q, D, Θ, and the natural variability, are shown in Figure S1. Results for bias-corrected data are shown in Figure S2.) The event and its analogues are characterised by an area of low z500 over Northern Europe and a band of high z500 over the Mediterranean and the western North Atlantic (Figure 2a). We observe significant decrease in z500 by about 25% in Western Europe (Figures 2d), with no variations found in either Sicily or Greece. A warming conditional to analogues is visible across most of the domain (Figure S1g). The atmospheric pattern of the factual period is further associated with increased FWI over Sicily and Greece (Figures 2f). There is a significant signal of decreasing winds over these regions (Figure S1m-p). The quality of the analogues Q (Figure S1q) shows that the z500 pattern is close to the median/average values of the Q distribution of its CF/F analogues, suggesting that the z500 pattern examined here is not unique and that we have confidence in our analysis. We detect a significant decrease in D, but no significant changes in Θ (Figure S1r, s). There is a slight shift towards an earlier occurrence of analogues in the factual period in terms of the seasonality (Figure S1t). The changes in

the large-scale modes of natural variability (Figure S1u-w) show a potential contribution from PDO. Finally, we observe an increase in analogues frequency of about one event per decade (Figure S1x).

For the CORDEX models, the average correlation coefficients between the ERA5 event-day z500 pattern and the model analogues are shown in Table S2. For this event, the average correlation ranges between 0.871 and 0.910. As all values are above the predefined threshold, all models are included in the ensemble. The change in z500 in the ERA5 validation analysis (Figure 2g) is similar to that of the full analysis (Figure 2d); both show a decrease in western Europe. The CORDEX ensemble suggests a weak decrease in the southwestern and southeastern parts of the domain and an increase in the eastern parts (Figure 2j). For t2m, ERA5 validation analysis (Figure 2n) shows a similar warming pattern as the full analysis (Figure 2h), and the model ensemble suggests significant warming over most of the domain (Figure 2k). FWI change in the validation analysis shows statistically significant increases in Sicily and Greece (Figure 2i), and so does the RCM ensemble (Figure 2l). Such similarity between the RCM ensemble and ERA5 suggests sufficient performance of the former for projecting future changes.

For the near future, a decrease in z500 is projected over the southern parts of the domain, covering both Sicily and Greece (Figure 2m). FWI shows significant increases in both areas (Figure 2o). In the far future, z500 shows a significant decrease over the Mediterranean Sea (Figure 2p), covering both areas of interest. FWI shows significant increases of considerable magnitude over most parts of western Europe; such increases are consistent among the ensemble members (Figure 2r). The average changes in FWI over the area most affected by the wildfire are shown in Figure 3 (results for bias-corrected data are shown in Figure S7). ERA5 shows average changes of 1.68 and 1.81 for the full and validation analyses, respectively. For the validation period, the CORDEX models suggest an ensemble-mean change of 2.18 (ensemble median of 2.3), which corresponds well with the ERA5 results. FWI over Sicily and Greece is projected to experience a mean increase of 3.11 and 9.32 (median of 2.75 and 9.63) in the near and far future, respectively.

3.2. 2022/07/12 France wildfires

In July 2022, Western Europe experienced a series of heatwaves, marked by record-breaking temperatures exceeding 40°C at multiple locations [36]. These high temperatures resulted from prolonged anticyclonic conditions and the influx of warm air from Morocco [37]. On July 12, 2022, two distinct forest fires erupted in the Bordeaux region of southwest France, specifically in Landiras and La Teste-de-Buch. They were exacerbated by moderate winds and ravaged more than 20,000 hectares of forested land, resulting in evacuation of 36,000 residents [38].

Figure 4 shows the results for the attribution of this event. (More for the ERA5 full analysis are shown in Figure S3. Results with bias correction are shown in Figure S4.) The salient features of the event were high z500 values over the British Isles and North-

Western Europe, an area of low z500 over Eastern Europe, and a small area of low z500 to the south-east of Iberia Figure 4a). We observe significant increases in z500 of about 50 m, in the region affected by wildfires (Figure 4j). The warming conditional to analogues is over 2 °C near the fire location (Figure 4e). The atmospheric pattern of the factual period is further associated with increased FWI in western France (Figure 4f). There is a signal of decreasing winds over the same region (Figure S3m-p). The quality of the analogues Q (Figure S3q) shows that z500 is higher than the median/average values of the Q distribution of its CF/F analogues, suggesting that this pattern is highly unusual. The results of our analysis should therefore be interpreted with caution. We do not detect any significant changes in D or Θ (Figure S3r, s). For the seasonal occurrence of analogues (Figure S3t), there is a slight shift of this type of events towards later seasons in the factual world. The changes in the natural variability (Figure S3u-w) highlight a potential contribution from ENSO and the PDO. Finally, we observe an increase in the analogues frequency of about one event more per decade (Figure S3x).

CORDEX models show less skill in simulating the z500 patterns for this event; the correlation coefficients range between 0.711 and 0.797 (Table S2). Given the predefined threshold, 30 models without bias correction and all models after bias correction are selected. For ERA5, the change in z500 in the validation analysis is similar to that of the full analysis; however, the significant increase over France is shifted to the northern Atlantic Ocean to the south of Portugal and Spain (Figure 4g). The change in t2m and FWI is shifted accordingly to lands near this area (Figure 4h, i). Over parts of southern France, increases in FWI can be identified (not significant). The patterns of changes of z500, t2m, and FWI in the CORDEX ensemble agree with the ERA5 ones (Figure 4j-l).

In the near future, z500 is projected to increase over the northern Atlantic Ocean, similar to the ERA5 pattern (Figure 4m). FWI shows significant increases over western Europe (Figure 4o). For the far future, z500 shows a decrease over parts of France (Figure 4p). FWI shows significant and substantial increases over western Europe, with agreement in the ensemble (Figure 4r). For the most affected areas (Figure 3), ERA5 shows average changes of 4.44 and 0.23 in FWI for the full and validation analyses, respectively. CORDEX ensemble shows a change comparable to the latter in the validation period. In the near and far future, FWI is projected to show ensemble-mean increases of 1.04 and 6.44 (ensemble median of 0.44 and 5.36), respectively.

3.3. 2018/07/16 Sweden wildfires

July 2018 is the hottest on record in Sweden, characterised by unusually warm and dry conditions [39]. This resulted in a high fire risk, and an unprecedented number of wildfires in Southern and Central Sweden. The largest of these ignited around July 12, and grew rapidly since July 16 [40]. Sweden activated the European Union's Civil Protection Mechanism, and received firefighting support from, amongst others, Denmark, France, and Italy [41].

Figure 5 shows the results for the Central Sweden wildfires of July 2018. (More

for the ERA5 full analysis is shown in Figure S5. Results for bias-corrected data are shown in Figure S6.) The event and its analogues are characterised by an area of high z500 over northern Scandinavia (Figure 5a). z500 has not changed markedly between the counterfactual and factual periods (Figure 5d). A warming conditional to analogues is of moderate magnitude near the location of the largest wildfires (Figure 5e). Conditioned on the analogues, significant increases in FWI can be identified over central Sweden (Figure 5f). For wind, no clear signal emerges at the wildfire location (Figure S5m-p). The quality of the analogues Q (Figure S5q) shows that the z500 pattern is close to the median/average values of the Q distribution of its CF/F analogues, suggesting that this event is not unique and that we have confidence in our analysis. We detect no significant changes in D and Θ (Figure S5r, s). There is no systematic shift in seasonal timing of the analogues (Figure S5t). The changes in the natural variability (Figure S5u-w) highlight a potential contribution from ENSO. Finally, we observe an increase in the analogues frequency of almost two events per decade (Figure S5x).

The CORDEX ensemble shows sufficient skill in simulating the z500 patterns similar to the event-day pattern in ERA5, with average correlation coefficients ranging between 0.842 and 0.928 (Table S2); therefore, 30(31) models without(with) bias correction are included in the ensemble. z500 does not show significant change over the domain in the validation analysis (Figure 5g), which is similar to the full analysis (Figure 5d). FWI, on the other hand, shows a significant decrease over southern Sweden (Figure 5i). The CORDEX ensemble does not show significant change in both variables (Figure 5j, l).

For the near future, a decrease in z500 can be found over southern parts of Sweden (Figure 5m), and an increase in FWI can be identified over its central parts (Figure 5o). In the far future, the models project a significant decrease in z500 near the center of the domain (Figure 5p), and a significant increase in FWI over parts of Sweden and Norway (Figure 5r). The models do not show high agreement for this event. For the most affected areas (Figure 3), ERA5 shows average changes of 3.46 and -1.56, respectively, for the full and validation analyses. The models show an ensemble-mean change of -0.13 (median of -0.24). The change in ERA5 is below the lower quartile of the CORDEX ensemble (-0.93), suggesting a possible overestimation in the models. The ensemble projects mean changes of 0.48 and 0.91 (median of 0.36 and 0.39) in the near and far future, respectively.

4. Discussion

The attribution of extreme weather events to climate change remains a challenging task due to the complex nature of the climate system and the limitations of available data. Our study adopts an approach based on atmospheric analogues and examines the atmospheric circulation associated with recent wildfires. For the events analysed here, we see no systematic shifts in the large-scale atmospheric pattern. In the French fires, we see a significant increase in z500 overlapping the location of the fires, while in the other two cases the significant changes are spatially limited and distant from the fire locations.

For the French wildfires, the higher z500 could be a contributing factor to the dry, hot conditions which characterised the event. In all three cases, we observe a warming of the analogues across large parts of the domain, which reflect the overarching background of global warming. The FWI of the analogues increased during the factual periods for all three cases. This demonstrates the strong connection between the atmospheric circulation patterns and the fire weather conditions for these three events.

Following the ClimaMeter approach, we further discuss the analogue quality. Two of the analysed cases – Sicily/Greece and Sweden – have a good analogue quality in both periods, suggesting high confidence in our analysis. For France, the analogues are of poor quality, suggesting that the event is highly unusual and that our results should be interpreted with care. In particular, in Figures S3a-c it is evident that the analogues miss the negative z500 anomaly in the south-western part of the domain. Moreover, possible contributions from large-scale modes of climate variability are observed for all three cases. Although we do not relate causally the observed changes in the meteorological fields to those in the distribution of the climate variability indices, we cannot exclude that these may have a modulating effect. At the same time, arguments have been made for the need to radically change the null hypothesis in attribution studies ([42]). That is, we should, by default, assume that observed changes are due to anthropogenic climate change, and only attribute them to other factors when this null hypothesis is disproved. Leveraging this perspective, we would attribute the observed changes in the fire weather to anthropogenic climate change, with a possible contribution from natural variability. In addition, when examining the analogues frequency for the entire period, we observe in all three cases a systematic increase. This points to atmospheric patterns similar to the ones associated with these impactful fire events becoming increasingly frequent with time. This is in qualitative agreement with the literature evidencing an increased wildfire risk in the historical period across several European regions [43].

To address the issue of limited data and to better understand the connection between extreme events and atmospheric circulation, the high-resolution CORDEX ensemble is employed. All models show high skill in simulating the event-day z500 pattern for the Sicily/Greece and Sweden events, but less skill for the France case, which could be due to the fact that the latter is highly unusual. From another perspective, it can also be considered that the models have faithfully reproduced the rarity (low analogue quality) of this event. The ensemble-mean changes in z500 and FWI in CORDEX models are similar to those obtained in ERA5, suggesting the models' ability to capture the connection between atmospheric circulation patterns and the fire weather conditions. On the other hand, in the validation analyses, less than 80% of the ensemble members agree on the sign of change in z500 and FWI for all three events, emphasizing the uncertainty in these variables among models. In the mid-21st century, the CORDEX ensemble projects significant decreases in z500 in and/or near the location of the wildfire for all three events. These are associated with significant and consistent increases in t2m over almost the entire domain and significant increases in FWI over the areas of interest. The decrease in z500 does not contradict the current consensus on a global

mean increasing trend [44], since this variable is detrended before the analogue search. This decrease may also be related to reduced relative humidity, which has been shown to decrease over the Mediterranean region [7, 5] and significantly impact fire weather conditions [45]. In the late 21st century, similar changes are projected, but with a larger magnitude and/or over a larger area. The ensemble members show a high agreement in their projected sign of change in FWI for the Sicily/Greece and France events in the late 21st century.

5. Conclusions

Our study attributed changes in atmospheric circulation patterns and associated surface variables during recent destructive wildfires in Sicily and Greece (2023), southwest France (2022) and Sweden (2018). We utilized the 500 hPa geopotential height field to identify analogues for past (factual) and recent (counterfactual) periods in the reanalysis, as well as under the present-day and future climate in a high-resolution RCM ensemble, providing a framework for studying changes in meteorological conditions favouring the occurrence of wildfires under climate change.

In all three cases, we find that differences between the two periods resulted in increased fire weather conditions. In other words, atmospheric patterns similar to those that coincided with the selected wildfire events correspond today to a higher fire weather index than they did in the past. This implies an increased wildfire hazard, given comparable atmospheric states. We attribute this to human-driven climate change, with natural variability possibly playing a contributing role. These attributable changes can be identified in the CORDEX ensemble. Conditioned on similar atmospheric patterns, the models project, with consistency, increases in fire weather index in the study areas in the future.

Our study underscores the challenges inherent to attributing extreme weather events and associated hazards – such as wildfires – to climate change. The intrinsic difficulty in isolating sources of natural variability, and the comparatively short observational period pose considerable hurdles. Nevertheless, the analysis performed here provides an initial framework by employing a high-resolution climate model ensemble to help further develop our understanding of the links between atmospheric circulation, climate change, and wildfires. This methodology could be included in the pipeline in ClimaMeter to improve the robustness of the attribution process.

Acknowledgments

D.F., E.C., and C.L. received support from the European Union's Horizon 2020 research and innovation programme under grant agreement No. 101003469 (XAIDA). D.F. and G.M. also received support from the Marie Sklodowska-Curie grant agreement No. 956396 (EDIPI). D.F. and T.A. acknowledge useful discussions within the MedCyclones COST Action (CA19109) and the FutureMed COST Action (CA22162) communities.

Author Contributions

D.F. and E.C. devised the study. C.L., R.N., D.F., and T.A. performed the analyses. All authors contributed to discussing and writing the paper.

Competing Interest

The authors declare no competing interests nor conflicts of interest. No human or animal data have been used in this study.

Data Availability

ERA5 is the latest climate reanalysis being produced by ECMWF as part of implementing the EU-funded Copernicus Climate Change Service (C3S), providing hourly data on atmospheric, land-surface and sea-state parameters together with estimates of uncertainty from 1979 to present day. ERA5 data are available on the C3S Climate Data Store on regular latitude-longitude grids at $0.25° \times 0.25°$ resolution have been downloaded from `https://cds.climate.copernicus.eu/#!/search?text=ERA5&type=dataset`, accessed on 2023-10-18. CORDEX is a part of the World Climate Research Program (WCRP) that aims to provide regional climate model data over various domains through coordinated efforts of assorted institutes over the world. EURO-CORDEX data used in this study are available on the Earth System Grid Federation (ESGF) platform (e.g., `https://esgf-node.ipsl.upmc.fr/projects/esgf-ipsl`). The data was accessed on 2024-02-07.

References

[1] Jolly W, Cochrane M, Freeborn P *et al.* 2015 *Nature Communications* **6** 7537

[2] National Interagency Fire Center 2013 Federal firefighting costs (suppression only) `https://www.nifc.gov/fireInfo/fireInfo_documents/SuppCosts.pdf`

[3] Bowman D M J S *et al.* 2009 *Science* **324** 481–484

[4] Moritz M A, Morais M E, Summerell L A, Carlson J M and Doyle J 2005 *Proceedings of the National Academy of Sciences of the United States of America* **102** 17912–17917

[5] Seneviratne S, Zhang X, Adnan M, Badi W, Dereczynski C, Di Luca A, Ghosh S, Iskandar I, Kossin J, Lewis S, Otto F, Pinto I, Satoh M, Vicente-Serrano S, Wehner M and Zhou B 2021 Weather and climate extreme events in a changing climate *Climate Change 2021: The Physical Science Basis. Contribution of Working Group I to the Sixth Assessment Report of the Intergovernmental Panel on Climate Change* ed Masson-Delmotte V, Zhai P, Pirani A, Connors S L, Péan C, Berger S, Caud N, Chen Y, Goldfarb L, Gomis M I, Huang M, Leitzell K, Lonnoy E, Matthews J B R, Maycock T K, Waterfield T, Yelekçi O, Yu R and Zhou B (Cambridge, UK and New York, NY, USA: Cambridge University Press) book section 11, pp 1513–1765 URL `https://www.ipcc.ch/report/ar6/wg1/downloads/report/IPCC_AR6_WGI_Chapter11.pdf`

[6] Ranasinghe R, Ruane A, Vautard R, Arnell N, Coppola E, Cruz F, Dessai S, Islam A, Rahimi M, Ruiz Carrascal D, Sillmann J, Sylla M, Tebaldi C, Wang W and Zaaboul R 2021 Climate

change information for regional impact and for risk assessment *Climate Change 2021: The Physical Science Basis. Contribution of Working Group I to the Sixth Assessment Report of the Intergovernmental Panel on Climate Change* ed Masson-Delmotte V, Zhai P, Pirani A, Connors S L, Péan C, Berger S, Caud N, Chen Y, Goldfarb L, Gomis M I, Huang M, Leitzell K, Lonnoy E, Matthews J B R, Maycock T K, Waterfield T, Yelekçi O, Yu R and Zhou B (Cambridge, UK and New York, NY, USA: Cambridge University Press) book section 12, pp 1767–1925 URL https://www.ipcc.ch/report/ar6/wg1/downloads/report/IPCC_AR6_WGI_Chapter12.pdf

[7] Doblas-Reyes F, Sörensson A, Almazroui M, Dosio A, Gutowski W, Haarsma R, Hamdi R, Hewitson B, Kwon W T, Lamptey B, Maraun D, Stephenson T, Takayabu I, Terray L, Turner A and Zuo Z 2021 Linking global to regional climate change *Climate Change 2021: The Physical Science Basis. Contribution of Working Group I to the Sixth Assessment Report of the Intergovernmental Panel on Climate Change* ed Masson-Delmotte V, Zhai P, Pirani A, Connors S L, Péan C, Berger S, Caud N, Chen Y, Goldfarb L, Gomis M I, Huang M, Leitzell K, Lonnoy E, Matthews J B R, Maycock T K, Waterfield T, Yelekçi O, Yu R and Zhou B (Cambridge, UK and New York, NY, USA: Cambridge University Press) book section 10, pp 1363–1512 URL https://www.ipcc.ch/report/ar6/wg1/downloads/report/IPCC_AR6_WGI_Chapter10.pdf

[8] 2019 *Nature Geosci* **12** 81

[9] Vautard R, Kadygrov N, Iles C, Boberg F, Buonomo E, Bülow K, Coppola E, Corre L, van Meijgaard E, Nogherotto R, Sandstad M, Schwingshackl C, Somot S, Aalbers E, Christensen O B, Ciarlo J M, Demory M E, Giorgi F, Jacob D, Jones R G, Keuler K, Kjellström E, Lenderink G, Levavasseur G, Nikulin G, Sillmann J, Solidoro C, Sørland S L, Steger C, Teichmann C, Warrach-Sagi K and Wulfmeyer V 2021 *Journal of Geophysical Research (Atmospheres)* **126** e2019JD032344

[10] van Oldenborgh G J, van der Wiel K, Kew S, Philip S, Otto F, Vautard R, King A, Lott F, Arrighi J, Singh R and van Aalst M 2021 *Climatic Change* **166** 13

[11] Reed K A, Wehner M F and Zarzycki C M 2022 *Nature Communications* **13** 1905

[12] Bellprat O, Guemas V, Doblas-Reyes F and Donat M G 2019 *Nature Communications* **10** 1732

[13] Strauss B H, Orton P M, Bittermann K, Buchanan M K, Gilford D M, Kopp R E, Kulp S, Massey C, Moel H d and Vinogradov S 2021 *Nature Communications* **12** 2720

[14] Cadiou C, Noyelle R, Malhomme N and Faranda D 2023 *Asia-Pacific Journal of Atmospheric Sciences* **59** 83–94

[15] Van Oldenborgh G J, Wehner M F, Vautard R, Otto F E L, Seneviratne S I, Stott P A, Hegerl G C, Philip S Y and Kew S F 2022 *Earth's Future* **10** e2021EF002271

[16] Venäläinen A *et al.* 2014 *Natural Hazards and Earth System Sciences* **14** 1477–1490

[17] Faranda D, Bourdin S, Ginesta M, Krouma M, Messori G, Noyelle R, Pons F and Yiou P 2022 *Weather and Climate Dynamics*

[18] Faranda D, Messori G, Coppola E, Alberti T, Vrac M, Pons F, Yiou P, Saint Lu M, Hisi A N S, Brockmann P, Dafis S, Mengaldo G and Vautard R 2024 *Weather and Climate Dynamics* **5** 959–983 URL https://wcd.copernicus.org/articles/5/959/2024/

[19] Hersbach H 2016 The era5 atmospheric reanalysis. *AGU fall meeting abstracts* vol 2016 pp NG33D–01

[20] Copernicus Climate Change Service C D S 2019 *Copernicus Climate Change Service (C3S) Climate Data Store (CDS)* DOI: 10.24381/cds.0e89c522

[21] Van Wagner C E 1987 Development and structure of the canadian forest fire weather index system Report 37 Canadian Forest Service Ottawa, Canada

[22] Vitolo C, Di Giuseppe F, Barnard C and et al 2020 *Sci Data* **7** 216

[23] Jacob D, Petersen J, B E *et al.* 2014 *Regional Environmental Change* **14** 563–578

[24] Coppola E, Nogherotto R, Ciarlo' J M, Giorgi F, van Meijgaard E, Kadygrov N, Iles C, Corre L, Sandstad M, Somot S, Nabat P, Vautard R, Levavasseur G, Schwingshackl C, Sillmann J, Kjellström E, Nikulin G, Aalbers E, Lenderink G, Christensen O B, Boberg F, Sørland S L, Demory M E, Bülow K, Teichmann C, Warrach-Sagi K and Wulfmeyer V 2021 *Journal of*

Geophysical Research: Atmospheres **126** e2019JD032356
[25] Jézéquel A, Yiou P and Radanovics S 2018 *Climate dynamics* **50** 1145–1159
[26] Reed K A, Wehner M F and Zarzycki C M 2022 *Nature communications* **13** 1905
[27] Michelangeli P A, Vrac M and Loukos H 2009 *Geophysical Research Letters* **36**
[28] Vrac M and Michelangeli P A 2021 *CDFt: Downscaling and Bias Correction via Non-Parametric CDF-Transform* r package version 1.2 URL https://CRAN.R-project.org/package=CDFt
[29] Benjamini Y and Hochberg Y 1995 *Journal of the Royal Statistical Society: Series B (Methodological)* **57** 289–300
[30] Wilks D S 2011 *Statistical methods in the atmospheric sciences* (Academic press)
[31] Wilks D S 2016 *Bulletin of the American Meteorological Society* **97** 2263 – 2273
[32] IPCC 2021 Summary for policymakers *Climate Change 2021: The Physical Science Basis. Contribution of Working Group I to the Sixth Assessment Report of the Intergovernmental Panel on Climate Change* ed Masson-Delmotte V, Zhai P, Pirani A, Connors S L, Péan C, Berger S, Caud N, Chen Y, Goldfarb L, Gomis M I, Huang M, Leitzell K, Lonnoy E, Matthews J B R, Maycock T K, Waterfield T, Yelekçi O, Yu R and Zhou B (Cambridge, UK and New York, NY, USA: Cambridge University Press) pp 1–31 URL https://www.ipcc.ch/report/ar6/wg1/downloads/report/IPCC_AR6_WGI_SPM.pdf
[33] Global wildfire information system gwis accessed on 2024-07-23 URL https://gwis.jrc.ec.europa.eu/
[34] Service T C C C 2023 European summer 2023: a season of contrasting extremes accessed on 2024-10-25 URL https://climate.copernicus.eu/european-summer-2023-season-contrasting-extremes
[35] Specified A N 2023 Sicily wracked by wildfire and soaring temperatures accessed on 2023-10-26 URL https://english.elpais.com/international/2023-07-27/sicily-wracked-by-wildfire-and-soaring-temperatures.html
[36] Copernicus climate change service - european state of the climate 2022 https://climate.copernicus.eu/esotc/2022 accessed on 2023-10-27
[37] Commission E, Centre J R, San-Miguel-Ayanz J, Durrant T, Boca R, Maianti P, Libertà G, Oom D, Branco A, De Rigo D, Ferrari D, Roglia E and Scionti N 2023 *Advance report on forest fires in Europe, Middle East and North Africa 2022* (Publications Office of the European Union)
[38] France: Emergency crews responding to wildfires in pyrenees-orientales department as of june 28, 2022 accessed on 2023-10-27 URL https://crisis24.garda.com/alerts/2022/06/france-emergency-crews-responding-to-wildfires-in-pyrenees-orientales-department-as-of-june-28
[39] Wilcke R A I, Kjellström E, Lin C, Matei D, Moberg A and Tyrlis E 2020 *Earth System Dynamics* **11** 1107–1121 URL https://esd.copernicus.org/articles/11/1107/2020/
[40] Krikken F, Lehner F, Haustein K, Drobyshev I and van Oldenborgh G J 2021 *Natural Hazards and Earth System Sciences* **21** 2169–2179 URL https://nhess.copernicus.org/articles/21/2169/2021/
[41] Guardian T 2018 The swedish town on the frontline of the arctic wildfires accessed on 2024-09-11 URL https://www.theguardian.com/world/2018/jul/30/the-swedish-town-on-the-frontline-of-the-arctic-wildfires
[42] Lloyd E A and Shepherd T G 2020 *Annals of the New York Academy of Sciences* **1469** 105–124 (*Preprint* https://nyaspubs.onlinelibrary.wiley.com/doi/pdf/10.1111/nyas.14308) URL https://nyaspubs.onlinelibrary.wiley.com/doi/abs/10.1111/nyas.14308
[43] Agency E E 2021 Forest fires in europe accessed on 2024-10-25 URL https://www.eea.europa.eu/en/analysis/indicators/forest-fires-in-europe?activeAccordion=
[44] Christidis N and Stott P A 2015 *Geophysical Research Letters* **42** 10,798–10,806 URL https://agupubs.onlinelibrary.wiley.com/doi/abs/10.1002/2015GL066669
[45] Nogherotto R, Raffaele F, Graziano G and Coppola E 2024 *Submitted*

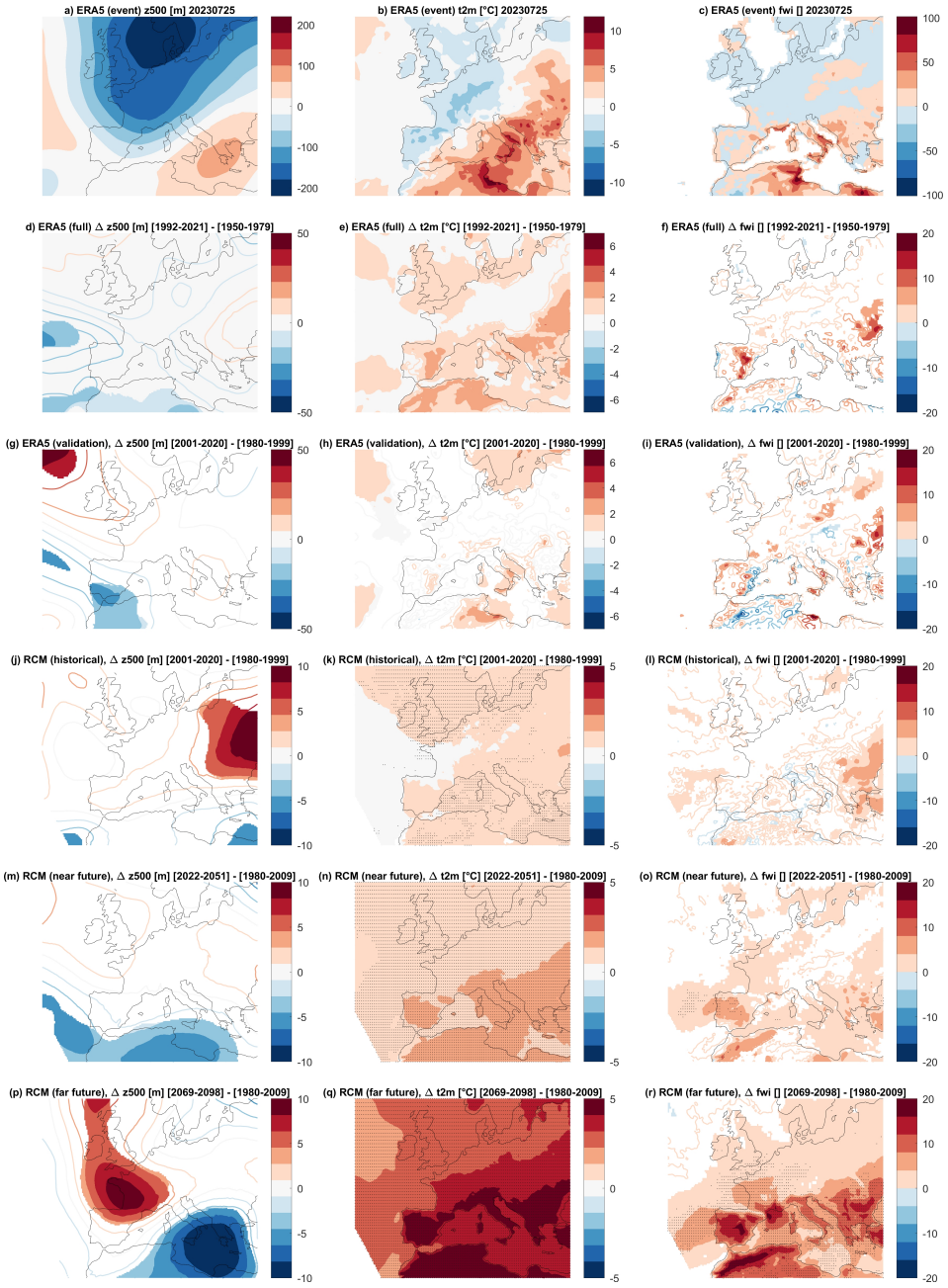

Figure 2. ERA5 and CORDEX ensemble Analogs analysis for the 2023/07/25 Sicily and Greece wildfires. Daily mean 500 hPa geopotential height z500 (a), 2-meter temperature t2m (b), and fire weather index FWI (c) on the day of the event. Δz500 (d), Δt2m (e), and ΔFWI (f) of the full analysis, between factual [1992-2021] and counterfactual periods [1950-1979]. Δz500 (g), Δt2m (h), and ΔFWI (i) of the validation analysis, between the factual [2001-2020] and counterfactual [1980-1999] periods. The corresponding Δz500 (j), Δt2m (k), and ΔFWI (l) of the historical period based on EURO-CORDEX ensemble. Δz500 (m, p), Δt2m (n, q), and ΔFWI (o, r) in the near [2022-2051] and far [2069-2098] future with respect to the reference period [1980-2009] based on EURO-CORDEX ensemble. Colored areas in (d-i) show significant anomalies with respect to the bootstrap procedure; colored areas in (j-r) show significant change based on two-sided t-tests; gray dots in (j-r) indicate that over 80% of the ensemble members agree on the sign of change. Note that color ranges are different for ERA5 and RCM analyses.

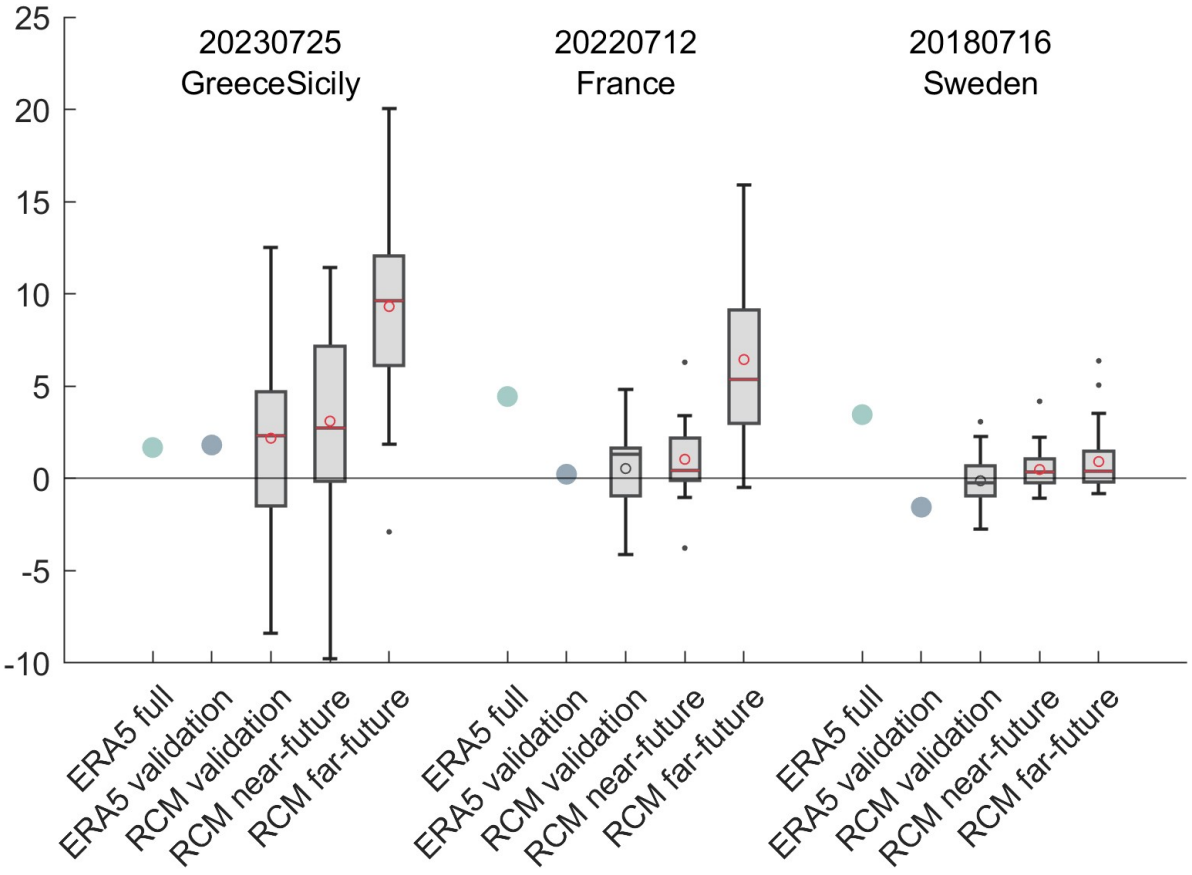

Figure 3. Boxplot for the area-averaged change over the boxes defined in Figure 1 for the three events. The green and blue filled circles indicate changes based on ERA5 full and validation analyses, respectively. The boxplots summarize the changes in the selected members of the EURO-CORDEX ensemble. The circles and lines inside the boxes indicate the mean and median, with the red color indicating statistical significance based on the one-sample t-tset and Wilcoxon signed rank test, respectively. The top and bottom edges of the boxes indicate the upper and lower quartiles; the dots indicate outliers that are more than 1.5 inter-quartile distance away from the top and bottom edges of the box. The labels on the x-axis indicate datasets/experiments.

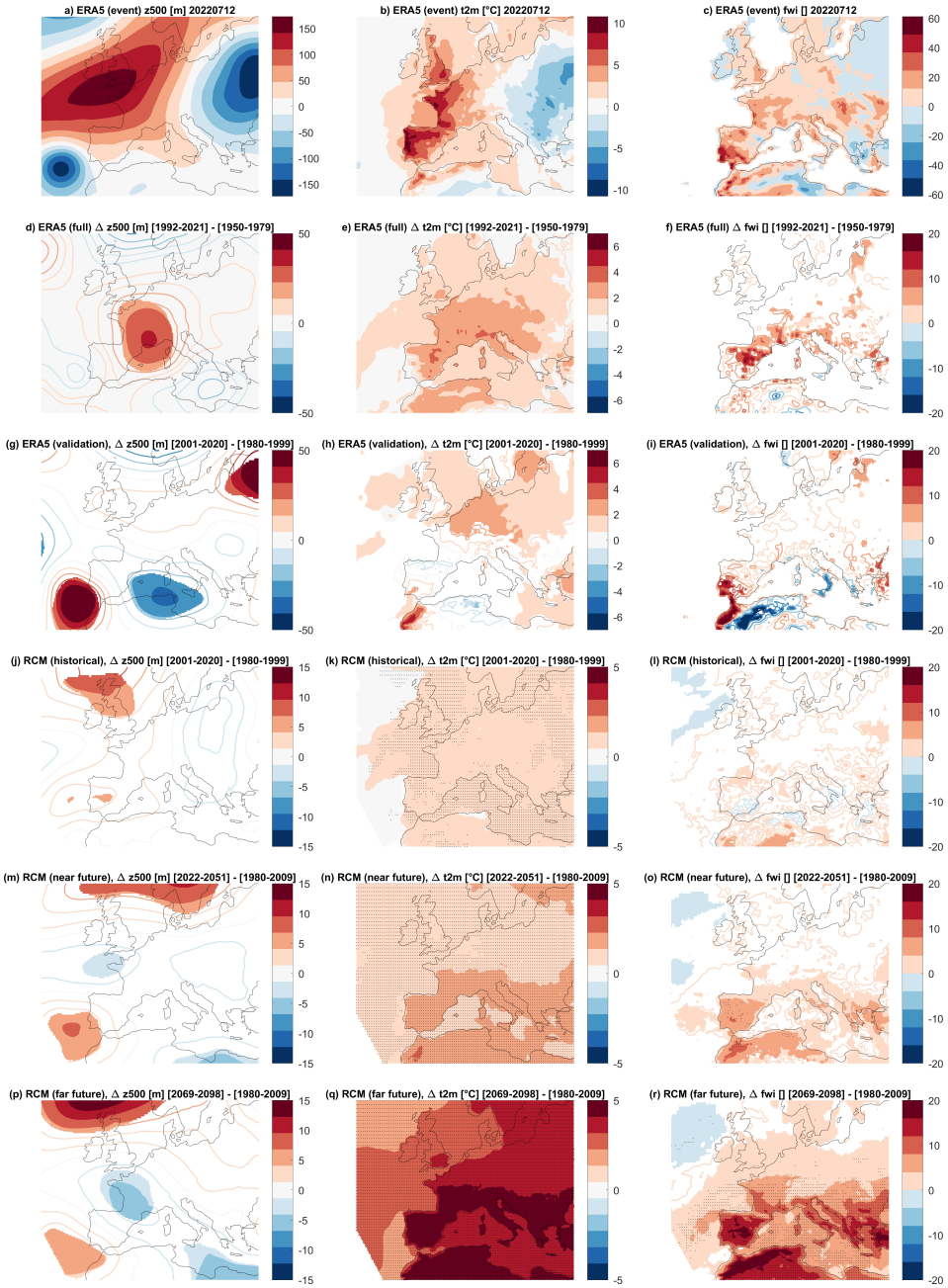

Figure 4. ERA5 and CORDEX ensemble Analogs analysis for the 2022/07/12 France wildfires. Daily mean 500 hPa geopotential height z500 (a), 2-meter temperature t2m (b), and fire weather index FWI (c) on the day of the event. Δz500 (d), Δt2m (e), and ΔFWI (f) of the full analysis, between factual [1992-2021] and counterfactual periods [1950-1979]. Δz500 (g), Δt2m (h), and ΔFWI (i) of the validation analysis, between the factual [2001-2020] and counterfactual [1980-1999] periods. The corresponding Δz500 (j), Δt2m (k), and ΔFWI (l) of the historical period based on EURO-CORDEX ensemble. Δz500 (m, p), Δt2m (n, q), and ΔFWI (o, r) in the near [2022-2051] and far [2069-2098] future with respect to the reference period [1980-2009] based on EURO-CORDEX ensemble. Colored areas in (d-i) show significant anomalies with respect to the bootstrap procedure; colored areas in (j-r) show significant change based on two-sided t-tests; gray dots in (j-r) indicate that over 80% of the ensemble members agree on the sign of change. Note that color ranges are different for ERA5 and RCM analyses.

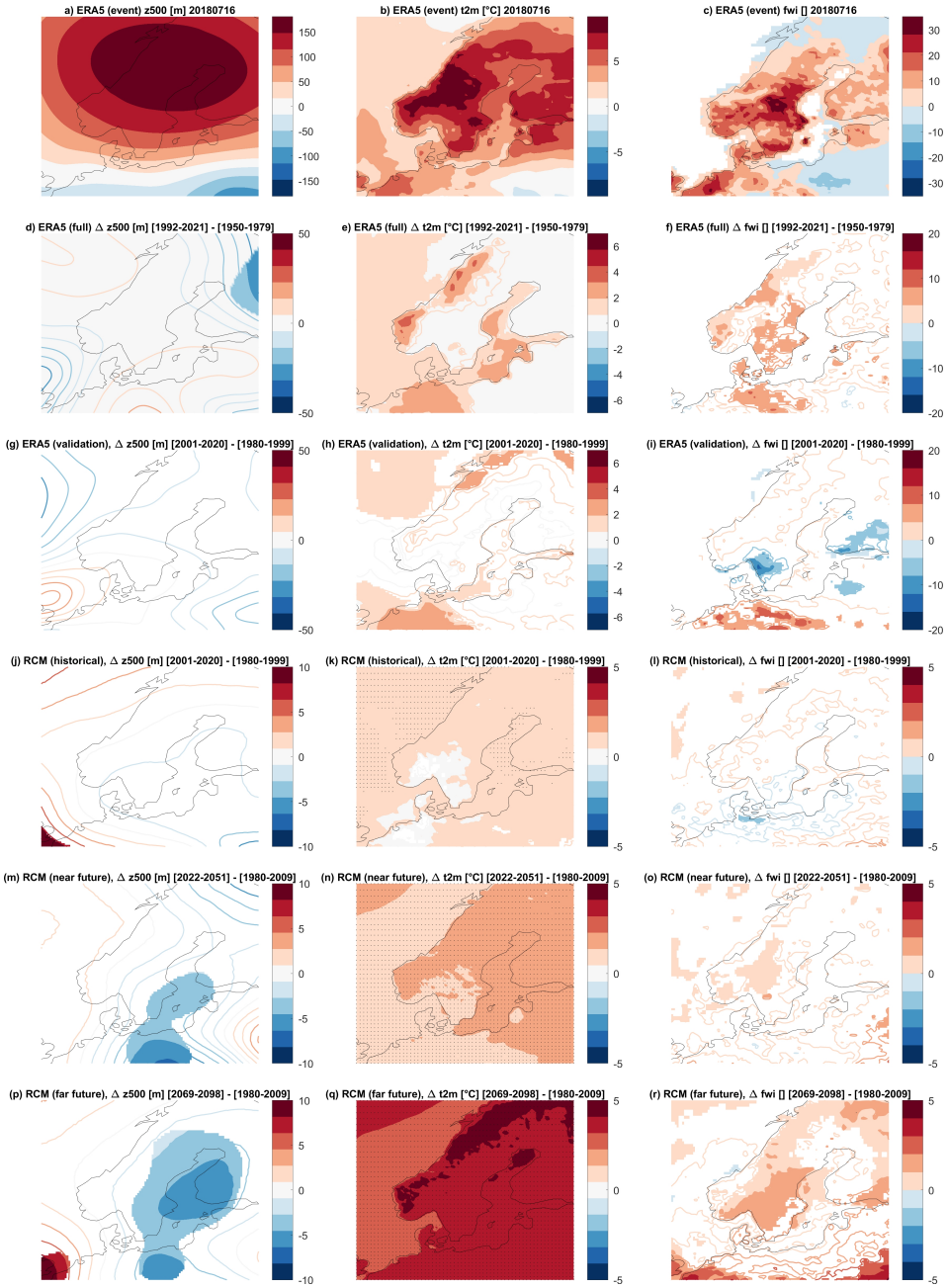

Figure 5. ERA5 and CORDEX ensemble Analogs analysis for the 2018/07/16 Central Sweden wildfires. Daily mean 500 hPa geopotential height z500 (a), 2-meter temperature t2m (b), and fire weather index FWI (c) on the day of the event. Δz500 (d), Δt2m (e), and ΔFWI (f) of the full analysis, between factual [1992-2021] and counterfactual periods [1950-1979]. Δz500 (g), Δt2m (h), and ΔFWI (i) of the validation analysis, between the factual [2001-2020] and counterfactual [1980-1999] periods. The corresponding Δz500 (j), Δt2m (k), and ΔFWI (l) of the historical period based on EURO-CORDEX ensemble. Δz500 (m, p), Δt2m (n, q), and ΔFWI (o, r) in the near [2022-2051] and far [2069-2098] future with respect to the reference period [1980-2009] based on EURO-CORDEX ensemble. Colored areas in (d-i) show significant anomalies with respect to the bootstrap procedure; colored areas in (j-r) show significant change based on two-sided t-tests; gray dots in (j-r) indicate that over 80% of the ensemble members agree on the sign of change. Note that color ranges are different for ERA5 and RCM analyses.

Supplemental Material for "Models Confirm that Recent European Wildfires Are Exacerbated by Anthropogenic Climate Change"

Chen Lu[1], Rita Nogherotto[1,2], Tommaso Alberti[3], Gabriele Messori[4], Erika Coppola[1], Davide Faranda[5,6,7]

[1] The Abdus Salam International Centre for Theoretical Physics, Trieste, Italy
[2] Istituto di Scienze Atmosferiche e Clima, CNR, Bologna, Italy
[3] Istituto Nazionale di Geofisica e Vulcanologia, Rome, Italy
[4] Department of Earth Sciences, Uppsala University, Uppsala, Sweden
[5] Laboratoire des Sciences du Climat et de l'Environnement, UMR 8212 CEA-CNRS-UVSQ, Université Paris-Saclay & IPSL, CE Saclay l'Orme des Merisiers, 91191, Gif-sur-Yvette, France
[6] London Mathematical Laboratory, 8 Margravine Gardens, London, W6 8RH, British Islands
[7] Laboratoire de Météorologie Dynamique/IPSL, École Normale Supérieure, PSL Research University, Sorbonne Université, École Polytechnique, IP Paris, CNRS, 75005, Paris, France

E-mail: clu@ictp.it

This Supplemental Material contains:

- Supplemental Text Sections
- Supplemental Tables S1-S2
- Supplemental Figures S1-S7

1. Procedure for the analogues analysis and tests for statistical significance

Before carrying out the analogues analysis, a linear trend is removed for each grid point of z500, to account for long-term thermodynamic trend. We also consider 2-meter temperature (t2m) and the 10-meter wind speed (wspd) during the identified analogues. For all variables, we deseasonalise the data by using a daily climatology defined as the average over a given calendar day across the full dataset.

The identification of analogues is based on computing the Euclidean distance $d(\mathbf{Ev}, \mathbf{Y})$ between the *target event* ($\mathbf{Ev}$) and the remaining set of latitude-longitude z500 maps ($\mathbf{Y}$). We select as analogues of $\mathbf{Ev}$ the best 22 patterns that minimize $d(\mathbf{Ev}, \mathbf{Y})$. These correspond to approximately 0.6% of days in the dataset. Previous analyses have shown a weak dependence of the results on the exact number of analogues chosen. We constrain our search to the extended season during which the *target event* occurred, as this helps ensure that other meteorological conditions beyond the z500 pattern remain similar to those of the *target event*. In this study, since all three events happened in summer, we search for analogues in the extended summer, i.e., June, July, August, and September. As conventional in attribution studies, the event itself is excluded. We also exclude a window of 3 days before and after the event. We also compute analogue quality Q, which is the average Euclidean distance between the *target event* and its 22 most similar analogs. Q can be used to determine how unique a *target event* is, and the level of confidence we can place in our analogues approach. If the Q value for $\mathbf{Ev}$ falls within the same distribution as its analogs, it implies that the event is not unique, allowing for attribution with a high degree of confidence. Conversely, if the Q value is in the upper tail of the distribution, the event largely unique and, consequently, unattributable.

Once analogues are identified, we compute their dynamical systems metrics instantaneous dimension D and persistence Θ [1, 2, 3, 4]. D is a proxy for the active number of degrees of freedom of a given atmospheric configuration, and hence is proportionally related to its intrinsic predictability. Θ is a measure of the clustering of similar consecutive atmospheric maps. When the dimension D of the *target event* is higher(lower) than that of its analogues, then it will be less(more) predictable than the closest dynamical situations identified in the data. When the persistence Θ of the *target event* is higher(lower) than that of its analogues, then it will be more(less) persistent than the closest dynamical situations identified in the data.

With the identified analogues, the composites in the counterfactual and factual periods, as well as the changes between the two, can be calculated. Statistical significance of the change is evaluated using a bootstrap procedure, in which the analogues of the two periods are pooled together; from it, 1,000 samples of 2 sets of 22 analogues are taken, representing the analogues for the counterfactual and factual periods, which are then used to calculate the changes. If the actual change of a grid point is more than 2 standard deviations above or below the mean of the bootstrap samples, it is then considered as statistically significant [5].

The analysis of the analogues provides an indication of differences between

the factual and counterfactual periods, but does not provide a direct indication of their cause. Observed changes could, in principle, be related to the influence of low-frequency modes of natural climate variability such as the El Niño-Southern Oscillation (ENSO), the Atlantic Multidecadal Oscillation (AMO) or the Pacific Decadal Oscillation. To account for this, we utilize monthly indices sourced from NOAA/ERSSTv5 data obtained from the Royal Netherlands Meteorological Institute (KNMI) Climate Explorer. To evaluate their impact on the *target event*, we test for significant changes between factual and counterfactual probability distribution functions (PDFs) using a two-tailed Cramér-von Mises test [6] at the 0.05 significance level. If the p-value falls below 0.05, we reject the null hypothesis ($H = 0$), signifying that both samples originate from distinct distributions, and the role of natural variability cannot be dismissed.

Additionally, we determine the top 54 analogues (approximately 0.6% of days) for the entire time interval and gauge a linear trend in the number of analogues per decade. To assess the significance of these trends, we determine their confidence intervals using the Wald method [7].

2. Detailed explanation of the Analogues Metrics

2.1. Predictability

The attractor of a dynamical system is a geometric object defined in the space hosting all the possible states of the system (phase-space). Each point ζ on the attractor can be characterized by two dynamical indicators: the local dimension D, which indicates the number of degrees of freedom active locally around ζ, and the persistence Θ, a measure of the mean residence time of the system around ζ [8].

D can be considered as a proxy for the active number of degrees of freedom of a given atmospheric configuration, and hence is proportionally related to its intrinsic predictability. When the dimension D of the *target event* is higher(lower) than that of its analogues, then it will be less(more) predictable than the closest dynamical situations identified in the data.

To determine D, we exploit recent results from the application of extreme value theory to Poincaré recurrences in dynamical systems. This approach considers long trajectories of a system — in our case successions of daily Z500 latitude–longitude maps — corresponding to a sequence of states on the attractor. For a given point ζ in phase space (e.g., a given Z500 map), we compute the probability that the system returns within a ball of radius ϵ centered on the point ζ. The [9] theorem, modified by [10], states that logarithmic returns:

$$g(x(t)) = -\log(\mathrm{dist}(x(t), \zeta)) \tag{1}$$

yield a probability distribution such that:

$$\Pr(z > s(q)) \simeq \exp\left[-\vartheta(\zeta)\left(\frac{z - \mu(\zeta)}{\sigma(\zeta)}\right)\right] \tag{2}$$

where $z = g(x(t))$ and s is a high threshold associated with a quantile q of the series $g(x(t))$. Requiring that the orbit falls within a ball of radius ϵ around the point ζ is equivalent to asking that the series $g(x(t))$ is over the threshold s; therefore, the ball radius ϵ is simply $e^{-s(q)}$. The resulting distribution is the exponential member of the Generalized Pareto Distribution family. The parameters μ and σ, namely the location and the scale parameter of the distribution, depend on the point ζ in phase space. $\mu(\zeta)$ corresponds to the threshold $s(q)$ while the local dimension $D(\zeta)$ can be obtained via the relation $\sigma = 1/D(\zeta)$. This is the metric of predictability introduced in the manuscript.

When $x(t)$ contains all the variables of the system, the estimation of D based on extreme value theory has a number of advantages over traditional methods (e.g., the box-counting algorithm [11, 12]). First, it does not require the estimation of the volume of different sets in scale space: the selection of $s(q)$ based on the quantile provides a selection of different scales s that depends on the recurrence rate around the point ζ. Moreover, it does not require the a priori selection of the maximum embedding dimension, as the observable g is always a univariate time-series.

2.2. Persistence

The persistence Θ is a measure of the clustering of similar consecutive atmospheric maps. When the persistence Θ of the *target event* is higher(lower) than that of its analogues, then it will be more(less) persistent than the closest dynamical situations identified in the data.

The persistence of the state ζ is measured via the extremal index $0 < \vartheta(\zeta) < 1$, an adimensional parameter, from which we extract $\Theta(\zeta) = \Delta t/\vartheta(\zeta)$. Here, Δt is the timestep of the dataset being analysed. $\Theta(\zeta)$ is therefore the average residence time of trajectories around ζ, namely the metric of persistence introduced in the manuscript, and it has unit of a time (in this study days). If ζ is a fixed point of the attractor, then $\Theta(\zeta) = \infty$. For a trajectory that leaves the neighborhood of ζ at the next time iteration, $\Theta = 1$. To estimate ϑ, we adopt the Süveges estimator [13]. For further details on the the extremal index, see [14].

2.3. Quality

Q is the average euclidean distance of a given day from its closest 22 analogs [15]. One can then compare Q for the targeted SLP or Z500 map to Q for each analogue of the target. If the value of Q for the targeted map belongs to the same distribution as, or is smaller than, the values of Q for the analogs, then the event has good analogs and attribution can be performed. If instead the Q for the targeted map is larger than that of the analogue days, then this indicates a highly unusual Z500 or SLP configuration and the results of the attribution analysis must be interpreted with care. Differences between the counterfactual and factual periods in the value of Q for the peak day of the targeted map indicate whether the the atmosphere is visiting states (analogs) that are more or less similar to the map associated with the extreme. Differences in the distribution of

Q for the 22 analogs indicate whether those states are in turn becoming more or less "typical" of the atmospheric variability. In order to test the homogeneity of the analogs in the two periods, we have computed Q for all days in the factual and counterfactual periods on the wide North Atlantic domain and applied the two-sided Cramér-von Mises test at the 0.05 significance level. The analogs quality diagnostic provides information on the fact that we have enough good and independent analogs to perform the analysis for the following reasons: i) the distance of the targeted maps from the analogs (dark dots in Figures S1, S3, S5(q)) is within the range of that of the analogs of the analogs. If we did not have good analogs the dots would lie outside of the violins for factual and counterfactual periods. ii) if the number of independent analogs for study would not be sufficient, the violin plots in Figures S1, S3, S5 (q) would not show a continuous distribution probability density function but rather consist of discontinuous and discrete patches.

References

[1] Freitas A C M, Freitas J M and Todd M 2011 *Journal of Statistical Physics* **142** 108–126

[2] Freitas A C M, Freitas J M and Vaienti S 2016 *arXiv preprint arXiv:1605.06287*

[3] Lucarini V, Faranda D, Freitas A C M, Freitas J M, Holland M, Kuna T, Nicol M, Todd M and Vaienti S 2016 *Extremes and recurrence in dynamical systems* (John Wiley & Sons) ISBN 1-118-63219-2

[4] Faranda D, Messori G, Alvarez-Castro M C and Yiou P 2017 *Nonlinear Processes in Geophysics* **24** 713–725

[5] Faranda D, Bourdin S, Ginesta M, Krouma M, Messori G, Noyelle R, Pons F and Yiou P 2022 *Weather and Climate Dynamics*

[6] Anderson T W 1962 *The Annals of Mathematical Statistics* 1148–1159

[7] Stein C and Wald A 1947 *The Annals of Mathematical Statistics* 427–433

[8] Faranda D, Messori G and Yiou P 2017 *Scientific reports* **7** 41278

[9] Freitas A C M, Freitas J M and Todd M 2010 *Probability Theory and Related Fields* **147** 675–710

[10] Lucarini V, Faranda D and Wouters J 2012 *Journal of statistical physics* **147** 63–73

[11] Liebovitch L S and Toth T 1989 *Physics Letters A* **141** 386–390 ISSN 0375-9601

[12] Sarkar N and Chaudhuri B B 1994 *IEEE Transactions on systems, man, and cybernetics* **24** 115–120

[13] Süveges M 2007 *Extremes* **10** 41–55

[14] Moloney N R, Faranda D and Sato Y 2019 *Chaos: An Interdisciplinary Journal of Nonlinear Science* **29** 022101

[15] Faranda D, Vrac M, Yiou P, Jézéquel A and Thao S 2020 *Geophysical Research Letters* **47** e2020GL088002

Number	GCM	Ensemble	RCM
1	CNRM-CERFACS-CNRM-CM5	r1	GERICS-REMO2015
2	CNRM-CERFACS-CNRM-CM5	r1	SMHI-RCA4
3	ICHEC-EC-EARTH	r12	CLMcom-ETH-COSMO-crCLIM-v1-1
4	ICHEC-EC-EARTH	r12	DMI-HIRHAM5
5	ICHEC-EC-EARTH	r12	KNMI-RACMO22E
6	ICHEC-EC-EARTH	r12	MOHC-HadREM3-GA7-05
7	ICHEC-EC-EARTH	r12	SMHI-RCA4
8	ICHEC-EC-EARTH	r1	DMI-HIRHAM5
9	ICHEC-EC-EARTH	r1	KNMI-RACMO22E
10	ICHEC-EC-EARTH	r1	SMHI-RCA4
11	ICHEC-EC-EARTH	r3	KNMI-RACMO22E
12	IPSL-IPSL-CM5A-MR	r1	GERICS-REMO2015
13	IPSL-IPSL-CM5A-MR	r1	KNMI-RACMO22E
14	MOHC-HadGEM2-ES	r1	CNRM-ALADIN63
15	MOHC-HadGEM2-ES	r1	ICTP-RegCM4-6
16	MOHC-HadGEM2-ES	r1	KNMI-RACMO22E
17	MOHC-HadGEM2-ES	r1	MOHC-HadREM3-GA7-05
18	MPI-M-MPI-ESM-LR	r1	CLMcom-ETH-COSMO-crCLIM-v1-1
19	MPI-M-MPI-ESM-LR	r1	CNRM-ALADIN63
20	MPI-M-MPI-ESM-LR	r1	DMI-HIRHAM5
21	MPI-M-MPI-ESM-LR	r1	ICTP-RegCM4-6
22	MPI-M-MPI-ESM-LR	r1	KNMI-RACMO22E
23	MPI-M-MPI-ESM-LR	r1	SMHI-RCA4
24	MPI-M-MPI-ESM-LR	r2	CLMcom-ETH-COSMO-crCLIM-v1-1
25	MPI-M-MPI-ESM-LR	r2	SMHI-RCA4
26	MPI-M-MPI-ESM-LR	r3	GERICS-REMO2015
27	MPI-M-MPI-ESM-LR	r3	SMHI-RCA4
28	NCC-NorESM1-M	r1	CLMcom-ETH-COSMO-crCLIM-v1-1
29	NCC-NorESM1-M	r1	GERICS-REMO2015
30	NCC-NorESM1-M	r1	KNMI-RACMO22E
31	NCC-NorESM1-M	r1	SMHI-RCA4

Table S1. List of EURO-CORDEX models used in the analysis.

Number	2023/07/25 Sicily-Greece		2022/07/12 France		2018/07/16 Sweden	
	Raw	Bias-corrected	Raw	Bias-corrected	Raw	Bias-corrected
1	0.876	0.882	0.724	0.739	0.895	0.893
2	0.871	0.871	0.748	0.760	0.902	0.901
3	0.901	0.903	0.747	0.742	0.915	0.914
4	0.892	0.891	0.769	0.771	0.915	0.907
5	0.896	0.889	0.746	0.749	0.924	0.923
6	0.896	0.894	0.759	0.755	0.922	0.918
7	0.895	0.891	0.763	0.755	0.906	0.910
8	0.905	0.891	0.755	0.756	0.923	0.919
9	0.897	0.892	0.711	0.713	0.917	0.912
10	0.909	0.898	0.740	0.746	0.928	0.921
11	0.894	0.890	0.751	0.752	0.919	0.912
12	0.890	0.883	0.792	0.787	0.914	0.908
13	0.896	0.875	0.789	0.797	0.912	0.904
14	0.887	0.884	0.777	0.779	0.909	0.903
15	0.889	0.879	0.751	0.761	0.920	0.918
16	0.884	0.878	0.775	0.772	0.916	0.913
17	0.889	0.879	0.788	0.783	0.919	0.906
18	0.895	0.888	0.768	0.767	0.842	0.877
19	0.894	0.899	0.774	0.769	0.902	0.907
20	0.895	0.890	0.777	0.773	0.905	0.897
21	0.888	0.892	0.747	0.748	0.916	0.923
22	0.899	0.895	0.766	0.767	0.865	0.893
23	0.894	0.890	0.777	0.770	0.890	0.885
24	0.901	0.895	0.778	0.774	0.901	0.901
25	0.905	0.898	0.766	0.766	0.908	0.915
26	0.907	0.900	0.770	0.773	0.900	0.912
27	0.907	0.902	0.761	0.761	0.897	0.907
28	0.910	0.895	0.742	0.740	0.910	0.908
29	0.904	0.888	0.781	0.790	0.890	0.899
30	0.905	0.896	0.761	0.754	0.890	0.878
31	0.905	0.900	0.760	0.762	0.922	0.902

Table S2. Average correlation coefficient between the event-day z500 pattern from ERA5 and the analogs identified in CORDEX simulations.

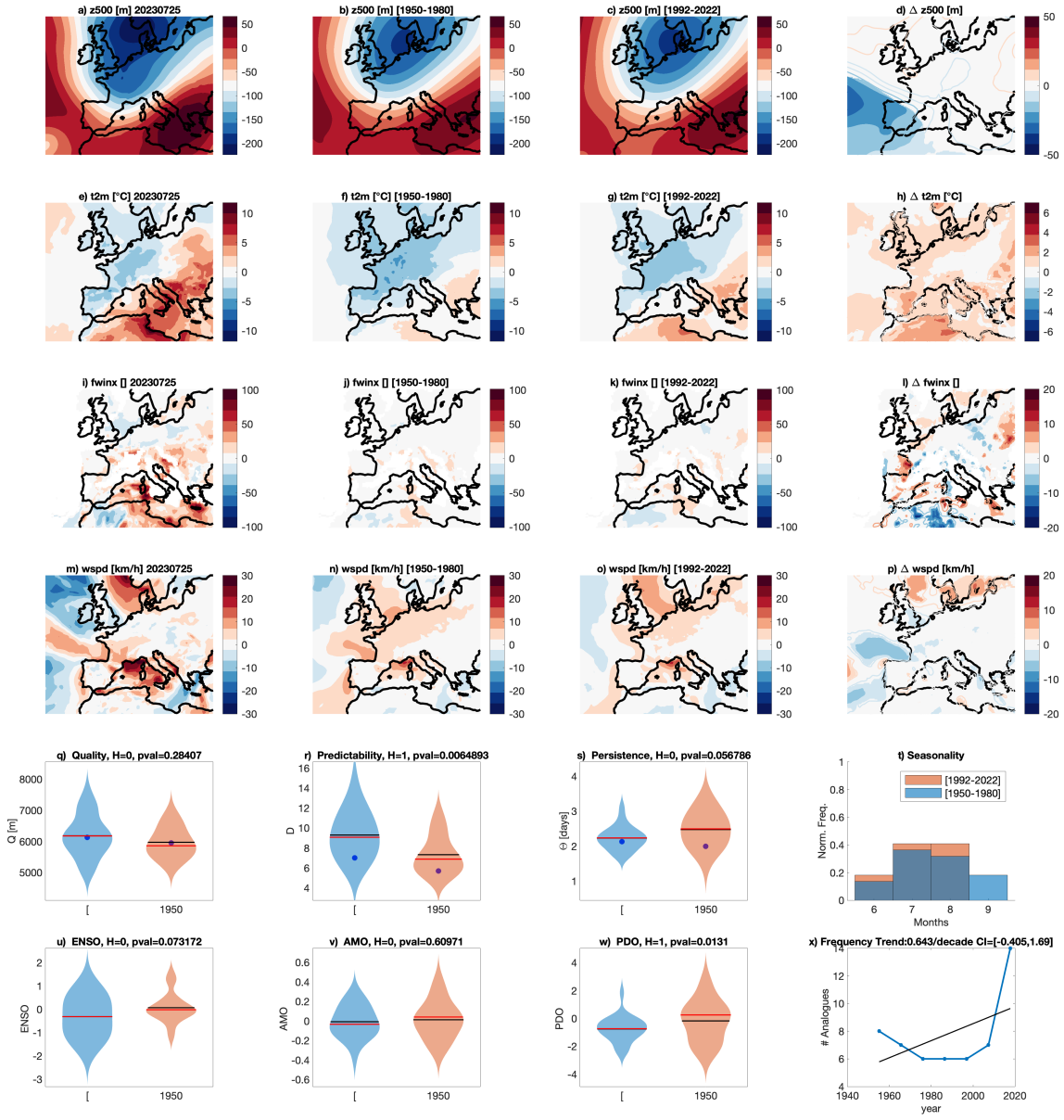

Figure S1. ERA5 Analogs analysis for the 2023/07/25 Sicily and Greece wildfires. Daily mean 500 hPa geopotential height z500 (a), 2-meter temperature t2m (e), fire weather index FWI (i), wind speed wspd (m) on the day of the event. Average of the 22 500 hPa geopotential height analogues found for the counterfactual [1950-1979] (b) and factual [1992-2021] (c) periods and corresponding 2-meter temperatures (f,g), fire weather index (j,k), and wind speed (n,o). Δz500 (d), Δt2m (h), ΔFWI (i), and Δwspd (p) between factual and counterfactual periods: colored areas show significant anomalies with respect to the bootstrap procedure . Violin plots for counterfactual (blue) and factual (orange) periods for the analogues Quality Q (q) the instantaneous dimension D (r), the persistence Θ (s) and the occurrence of analogues in each month (t). Violin plots for counterfactual (blue) and factual (orange) periods for ENSO (u), AMO (v), PDO (w). The number of analogues per decade (blue) and its linear trend (black; x). Values for the peak day of the extreme event are marked by a dot. Titles in (q–s and u—w) report the results of the Cramer-von Mises test H and the p-value pval. The title in panel (w) includes the value of the linear trend slope and its confidence interval CI in square brackets.

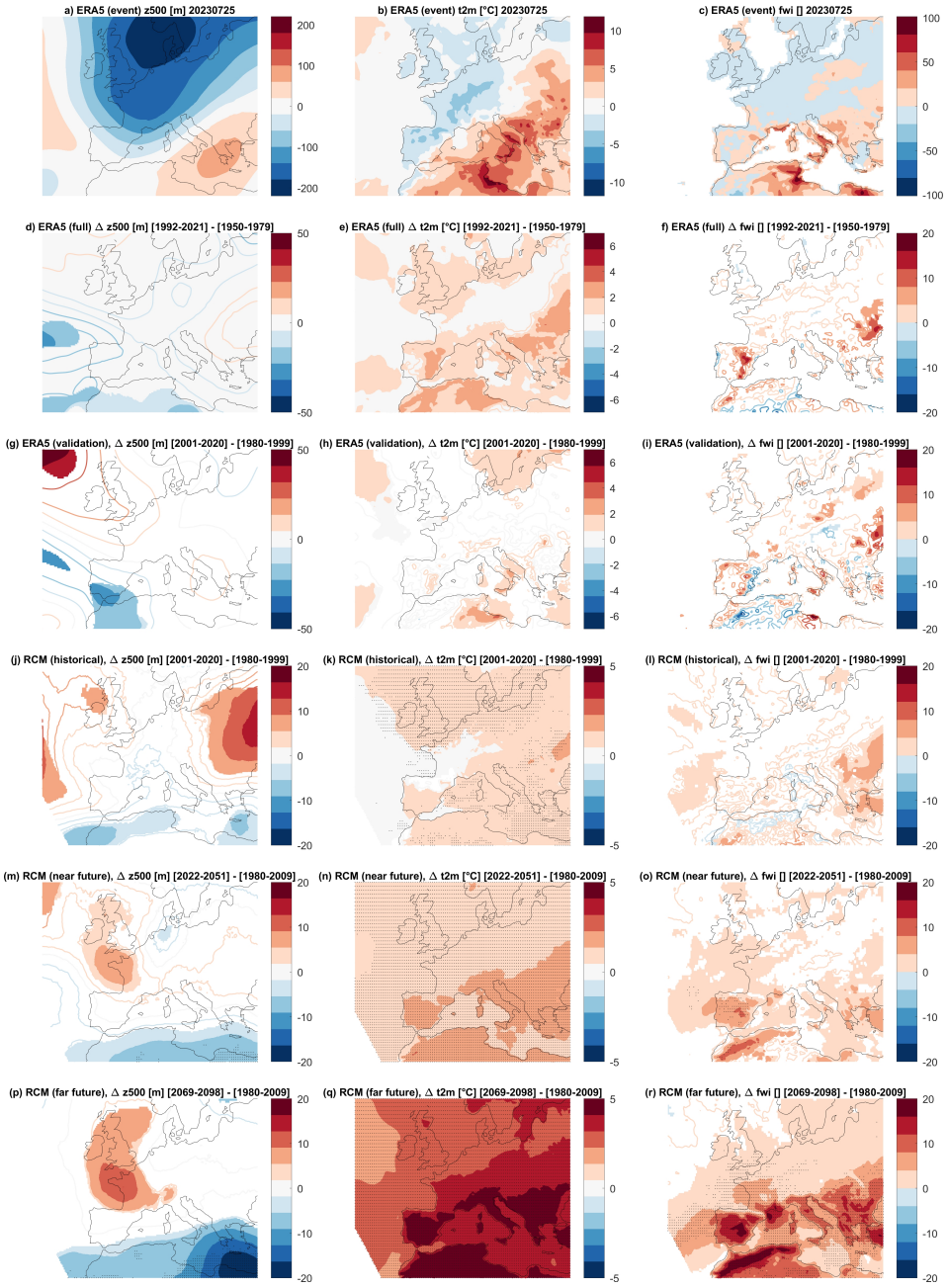

Figure S2. ERA5 and bias-corrected CORDEX ensemble Analogs analysis for the 2023/07/25 Sicily and Greece wildfires. Daily mean 500 hPa geopotential height z500 (a), 2-meter temperature t2m (b), and fire weather index FWI (c) on the day of the event. Δz500 (d), Δt2m (e), and ΔFWI (f) of the full analysis, between factual [1992-2021] and counterfactual periods [1950-1979]. Δz500 (g), Δt2m (h), and ΔFWI (i) of the validation analysis, between the factual [2001-2020] and counterfactual [1980-1999] periods. The corresponding Δz500 (j), Δt2m (k), and ΔFWI (l) of the historical period based on bias-corrected EURO-CORDEX ensemble. Δz500 (m, p), Δt2m (n, q), and ΔFWI (o, r) in the near [2022-2051] and far [2069-2098] future with respect to the reference period [1980-2009] based on bias-corrected EURO-CORDEX ensemble. Colored areas in (d-i) show significant anomalies with respect to the bootstrap procedure; colored areas in (j-r) show significant change based on two-sided *t*-tests; gray dots in (j-r) indicate that over 80% of the ensemble members agree on the sign of change. Note that color ranges are different for ERA5 and RCM analyses.

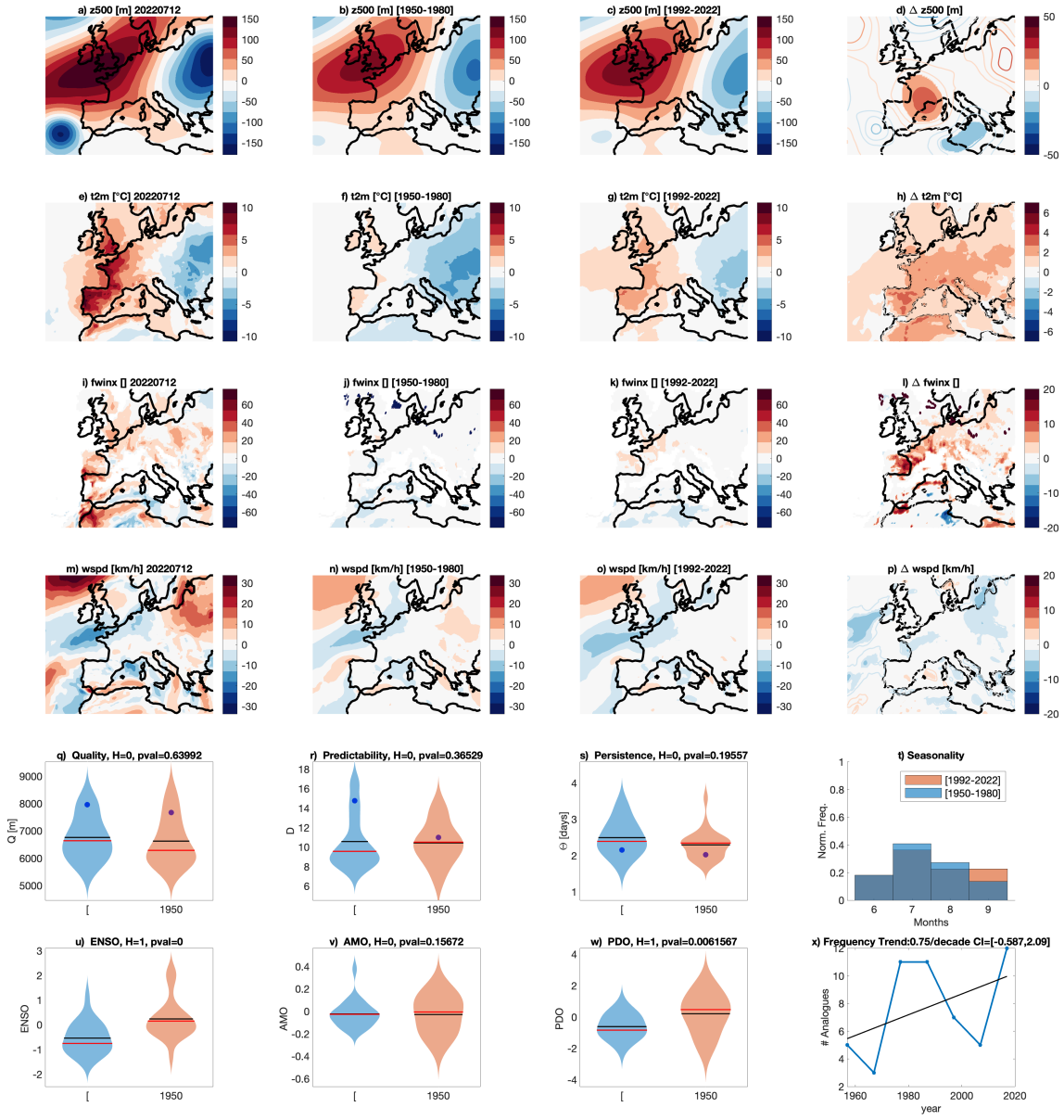

Figure S3. ERA5 Analogs analysis for the 2022/07/12 France wildfires. Daily mean 500 hPa geopotential height z500 (a), 2-meter temperature t2m (e), fire weather index FWI (i), wind speed wspd (m) on the day of the event. Average of the 22 500 hPa geopotential height analogues found for the counterfactual [1950-1979] (b) and factual [1992-2021] (c) periods and corresponding 2-meter temperatures (f,g), fire weather index (j,k), and wind speed (n,o). Δz500 (d), Δt2m (h), ΔFWI (i), and Δwspd (p) between factual and counterfactual periods: colored areas show significant anomalies with respect to the bootstrap procedure. Violin plots for counterfactual (blue) and factual (orange) periods for the analogues Quality Q (q) the instantaneous dimension D (r), the persistence Θ (s) and the occurrence of analogues in each month (t). Violin plots for counterfactual (blue) and factual (orange) periods for ENSO (u), AMO (v), PDO (w). The number of analogues per decade (blue) and its linear trend (black; x). Values for the peak day of the extreme event are marked by a dot. Titles in (q–s and u—w) report the results of the Cramer-von Mises test H and the p-value pval. The title in panel (w) includes the value of the linear trend slope and its confidence interval CI in square brackets.

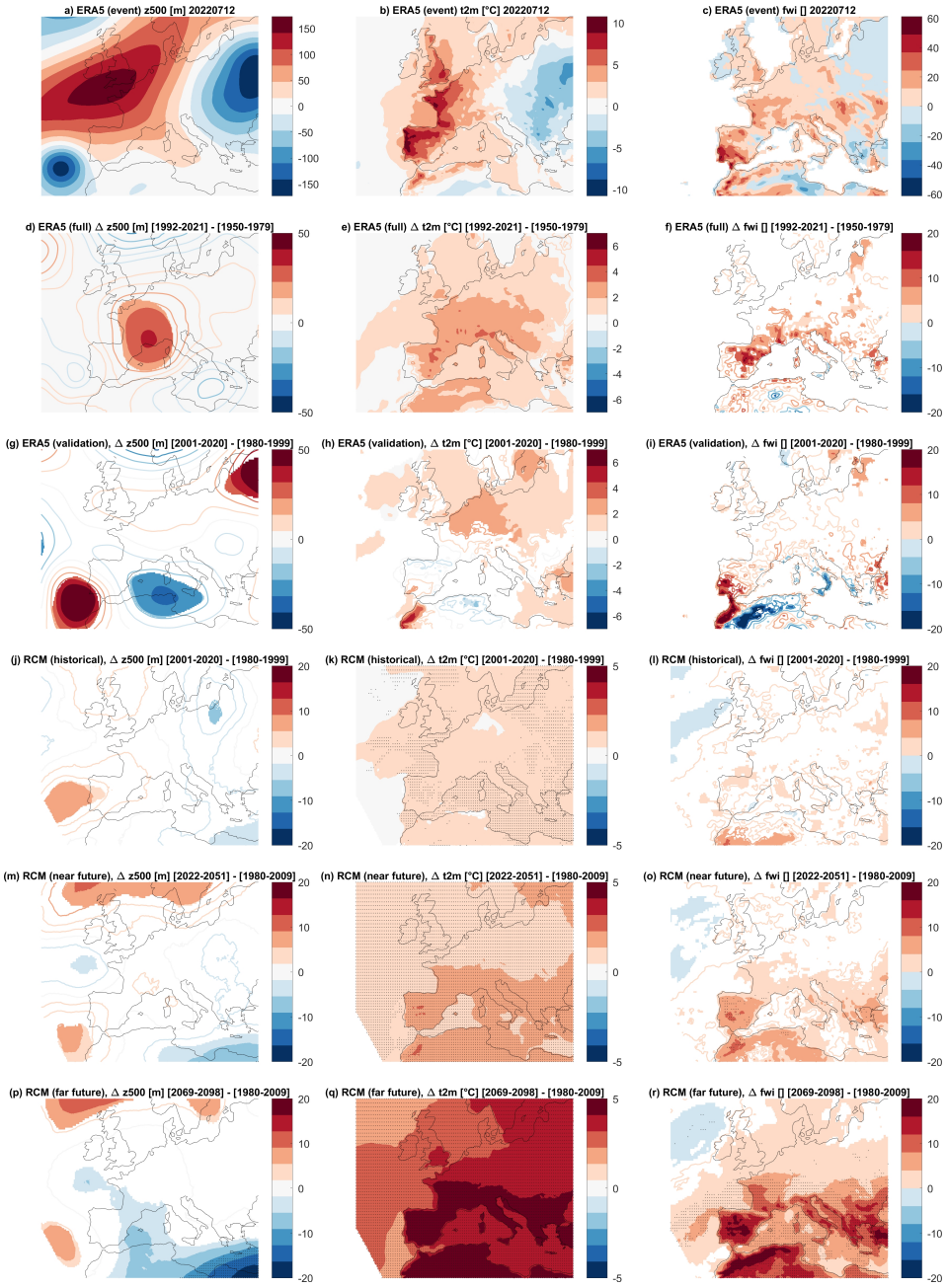

Figure S4. ERA5 and bias-corrected CORDEX ensemble Analogs analysis for the 2022/07/12 France wildfires. Daily mean 500 hPa geopotential height z500 (a), 2-meter temperature t2m (b), and fire weather index FWI (c) on the day of the event. Δz500 (d), Δt2m (e), and ΔFWI (f) of the full analysis, between factual [1992-2021] and counterfactual periods [1950-1979]. Δz500 (g), Δt2m (h), and ΔFWI (i) of the validation analysis, between the factual [2001-2020] and counterfactual [1980-1999] periods. The corresponding Δz500 (j), Δt2m (k), and ΔFWI (l) of the historical period based on bias-corrected EURO-CORDEX ensemble. Δz500 (m, p), Δt2m (n, q), and ΔFWI (o, r) in the near [2022-2051] and far [2069-2098] future with respect to the reference period [1980-2009] based on bias-corrected EURO-CORDEX ensemble. Colored areas in (d-i) show significant anomalies with respect to the bootstrap procedure; colored areas in (j-r) show significant change based on two-sided *t*-tests; gray dots in (j-r) indicate that over 80% of the ensemble members agree on the sign of change. Note that color ranges are different for ERA5 and RCM analyses.

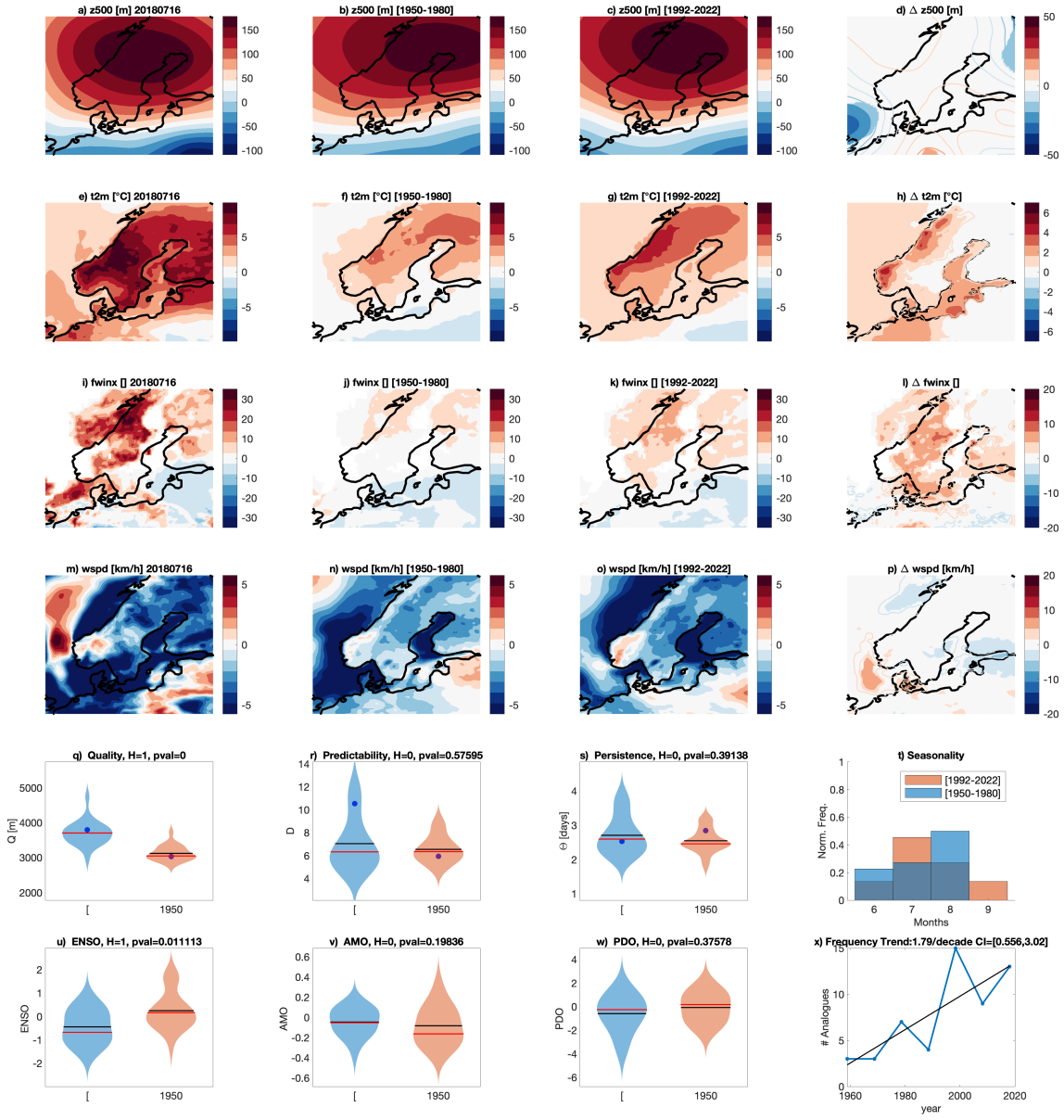

Figure S5. ERA5 Analogs analysis for the 2018/07/16 Central Sweden wildfires. Daily mean 500 hPa geopotential height z500 (a), 2-meter temperature t2m (e), fire weather index FWI (i), wind speed wspd (m) on the day of the event. Average of the 22 500 hPa geopotential height analogues found for the counterfactual [1950-1979] (b) and factual [1992-2021] (c) periods and corresponding 2-meter temperatures (f,g), fire weather index (j,k), and wind speed (n,o). Δz500 (d), Δt2m (h), ΔFWI (i), and Δwspd (p) between factual and counterfactual periods: colored areas show significant anomalies with respect to the bootstrap procedure . Violin plots for counterfactual (blue) and factual (orange) periods for the analogues Quality Q (q) the instantaneous dimension D (r), the persistence Θ (s) and the occurrence of analogues in each month (t). Violin plots for counterfactual (blue) and factual (orange) periods for ENSO (u), AMO (v), PDO (w). The number of analogues per decade (blue) and its linear trend (black; x). Values for the peak day of the extreme event are marked by a dot. Titles in (q–s and u—w) report the results of the Cramer-von Mises test H and the p-value pval. The title in panel (w) includes the value of the linear trend slope and its confidence interval CI in square brackets.

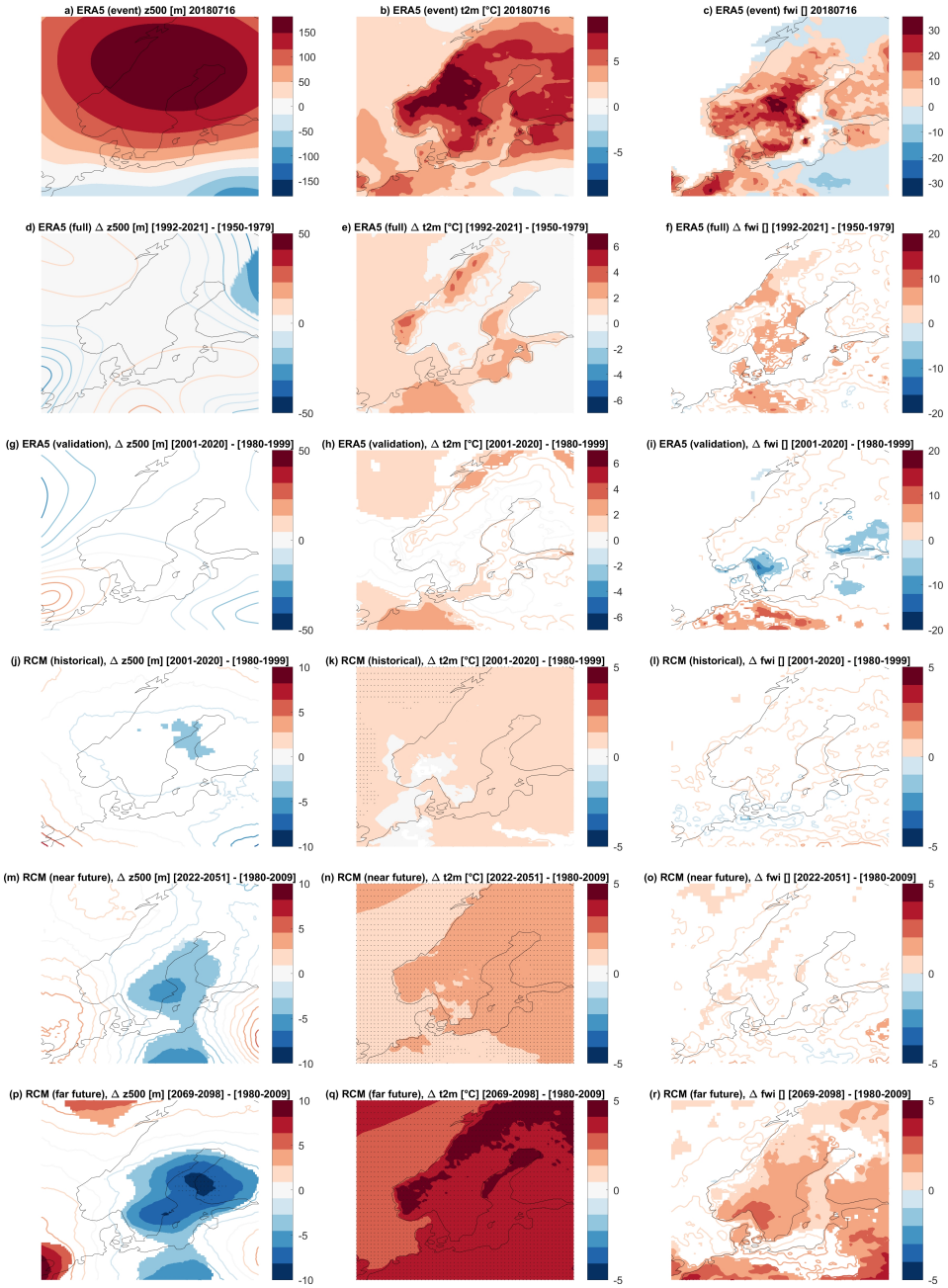

Figure S6. ERA5 and bias-corrected CORDEX ensemble Analogs analysis for the 2018/07/16 Central Sweden wildfires. Daily mean 500 hPa geopotential height z500 (a), 2-meter temperature t2m (b), and fire weather index FWI (c) on the day of the event. Δz500 (d), Δt2m (e), and ΔFWI (f) of the full analysis, between factual [1992-2021] and counterfactual periods [1950-1979]. Δz500 (g), Δt2m (h), and ΔFWI (i) of the validation analysis, between the factual [2001-2020] and counterfactual [1980-1999] periods. The corresponding Δz500 (j), Δt2m (k), and ΔFWI (l) of the historical period based on bias-corrected EURO-CORDEX ensemble. Δz500 (m, p), Δt2m (n, q), and ΔFWI (o, r) in the near [2022-2051] and far [2069-2098] future with respect to the reference period [1980-2009] based on bias-corrected EURO-CORDEX ensemble. Colored areas in (d-i) show significant anomalies with respect to the bootstrap procedure; colored areas in (j-r) show significant change based on two-sided *t*-tests; gray dots in (j-r) indicate that over 80% of the ensemble members agree on the sign of change. Note that color ranges are different for ERA5 and RCM analyses.

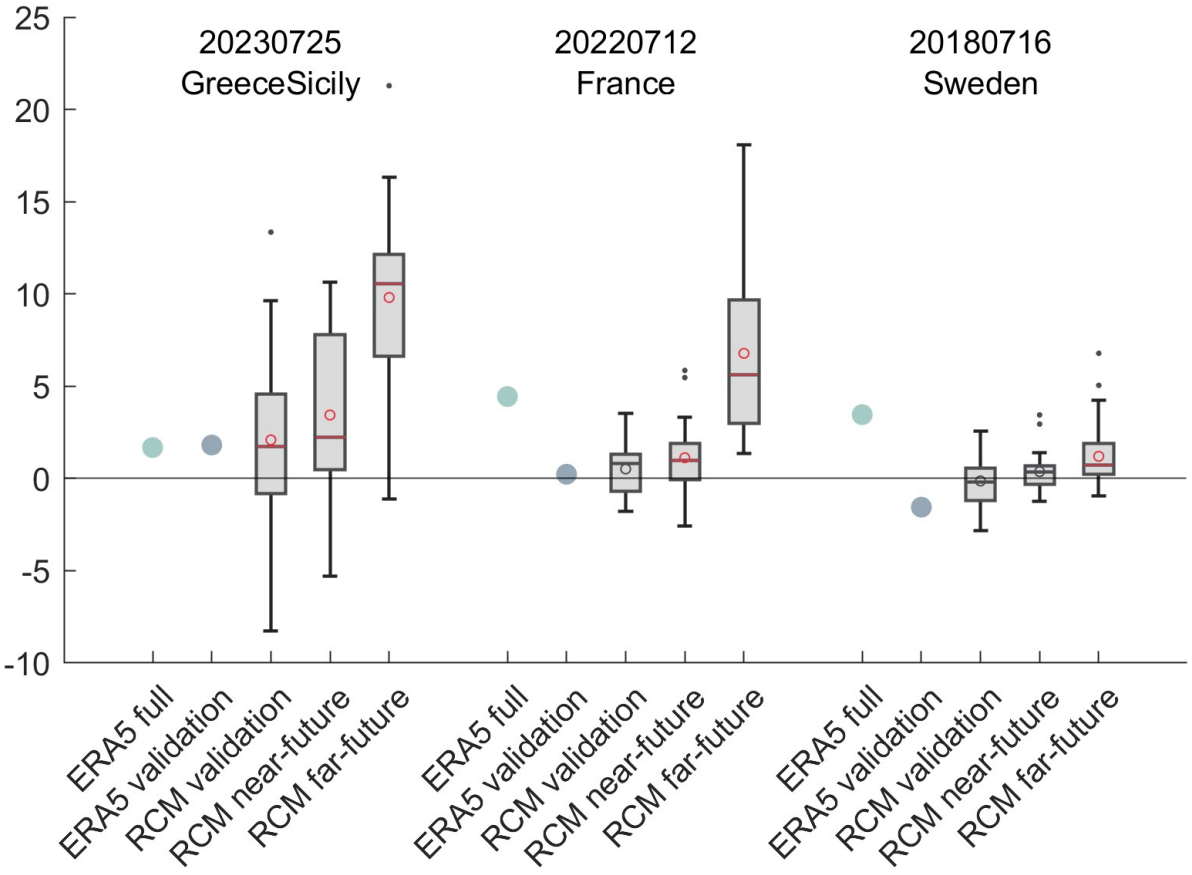

Figure S7. Boxplot for the area-averaged change over the boxes defined in Figure 1 for the three events. The green and blue filled circles indicate changes based on ERA5 full and validation analyses, respectively. The boxplots summarize the changes in the selected members of the bias-corrected EURO-CORDEX ensemble. The circles and lines inside the boxes indicate the mean and median, with the red color indicating statistical significance based on the one-sample t-tset and Wilcoxon signed rank test, respectively. The top and bottom edges of the boxes indicate the upper and lower quartiles; the dots indicate outliers that are more than 1.5 inter-quartile distance away from the top and bottom edges of the box. The labels on the x-axis indicate datasets/experiments.